have revealed that HA positively regulates proliferation, invasion, cell motility, multidrug resistance, and epithelial–mesenchymal transition in many tumor cell lines in vitro and in vivo (reviewed in ref. 23). Furthermore, an HAS inhibitor, 4-methylubelliferon, has been shown to decrease tumor proliferation and metastasis (25, 26).

Despite the importance of HA in tumorigenesis, assessing the role of circulating HA in tumor progression is difficult, because HA administered in the body is rapidly eliminated from the bloodstream (1). In this study, we generated Stab2 KO mice in which plasma HA levels were significantly elevated without any overt phenotype. Unexpectedly, tumor metastasis was markedly suppressed in these mice. We also found that administration of an anti-Stab2 antibody in WT mice elevated circulating HA levels and prevented tumor metastasis. Finally, we found that administration of a high dose of HA prevented the attachment of melanoma cells to the lungs in vivo and in vitro, and examined a possible link between circulating HA levels and tumor metastasis.

Results

Elevation of Circulating HA Levels in Stab2 KO Mice.

To address the physiological roles of Stab2 in vivo, we generated a Stab2 KO mouse line by replacing most of the first exon, including the ATG initiation codon and the first intron, with the LacZ and neomycin resistance genes (Figs. S1 A–C). The lack of Stab2 expression in KO mice was confirmed by RT-PCR and immunostaining (Figs. S1 D and H and S2D), Stab2-deficient mice were born according to the Mendelian ratio, grew normally, and showed no apparent abnormalities (Fig. S1 E and F). Histological analyses revealed no significant changes (Fig. S1G). Staining of liver sections with the anti-CD31 antibody, which binds HSECs as well as other types of ECs in the liver, demonstrated normal development of HSECs (Fig. S1H). Furthermore, we found no significant differences in conventional diagnostic markers for functions of the pancreas, liver, and kidney (Table S1). These results indicate that Stab2 is dispensable for normal development and viability in mice.

Given that Stab2 is a known scavenger receptor that binds and eliminates from the circulation various substances, including HA, ac-LDL, and heparin (4, 27, 28), we assessed the circulating levels of these substances in Stab2 KO mice. Although serum levels of ac-LDL and heparin were unchanged in the Stab2 KO mice (Table S1), serum HA levels were dramatically increased, by as much as 59-fold over control values (Fig. 1A). Because HA's molecular size affects its function (16), we next analyzed
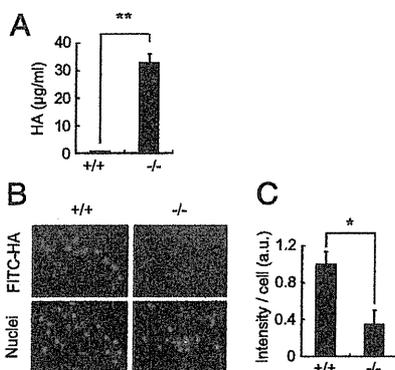
the molecular size of serum HA by electrophoresis using Stains-All (which stains negatively charged molecules), and estimated it as ~40 kDa (Fig. S1J). Given that >90% of the circulating HA is cleared by HSECs (1), and that Stab2 is specifically expressed in HSECs, we examined whether the high serum HA levels in Stab2 KO mice were due to impaired endocytosis. We prepared HSECs from WT and Stab2 KO mice and quantitatively evaluated their endocytotic activity based on the internalization of FITC-labeled HA and DiI-labeled ac-LDL (DiI-Ac-LDL) (Fig. 1B and C and Fig. S1 K and L). Although there was no significant difference in the internalization of DiI-Ac-LDL between WT and Stab2 KO mice, the internalization of HA into Stab2-deficient HSECs was markedly decreased, to only ~8% of the WT level. We also examined the expression of other HA receptors (CD44 and Lyve-1) and HA synthases (HAS1, HAS2, and HAS3) that can potentially affect HA levels, but found no significant changes in the Stab2 KO mice (Fig. S2 A and B). These results provide clear evidence that Stab2 is the major clearance receptor for HA in the body.

Metastasis of Melanoma Cells Is Suppressed in Stab2 KO Mice.

The elevation in serum HA levels in Stab2 KO mice prompted us to examine whether the lack of Stab2 has any effects on tumorigenesis. B16 melanoma cells are known to form tumor nodules in the lung when injected i.v. We administered B16F10 cells i.v. in littermates of Stab2$^{+/+}$ and Stab2$^{-/-}$ mice. After 14 d, numerous black nodules had formed on the lung surfaces of the Stab2$^{+/+}$ mice, but surprisingly, nodular formation was markedly reduced in Stab2$^{-/-}$ mice (Fig. 2 A and B). In contrast, tumor formation resulting from the s.c. inoculation of melanoma cells did not differ significantly between the Stab2$^{+/+}$ and Stab2$^{-/-}$ mice (Fig. 2C). Moreover, our in vitro experiments showed that the proliferation of B16F10 cells was not affected by HA, and a cell cycle analysis of B16F10 cells recovered from lung tumors revealed no difference between the Stab2 KO and WT mice (Fig. S3A). These results indicate that the metastasis, but not the proliferation, of melanoma cells was affected by the lack of Stab2.

To analyze the early stages of metastasis, we also conducted imaging in vivo, because the nodules of B16F10 cells at day 7 were too small to count. B16F10 cells were stably transfected with the firefly luciferase gene to generate B16F10-luc-G5 cells,
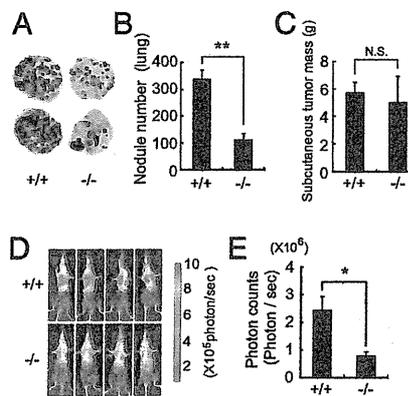

Fig. 1. Serum HA levels and internalization of HA in Stab2-deficient cells. (A) Serum HA levels in WT ($^{+/+}$) and homozygous ($^{-/-}$) littermates (n = 3; **P < 0.01). (B) Internalization of FITC-HA in Percoll-purified HSECs from Stab2$^{+/+}$ and Stab2$^{-/-}$ littermates. (Upper) Fluorescence of FITC-HA incorporated into cells. (Lower) Hoechst 33342 staining. (C) Quantification of FITC fluorescence intensity (n = 4; *P < 0.05).

Fig. 2. Homing of B16F10 melanoma to the lungs in Stab2 KO mice. B16F10 cells (5 × 10^5) were injected via the tail vein in Stab2$^{+/+}$ and Stab2$^{-/-}$ littermates. (A) Metastatic nodules formed on the lungs at day 14 after the injection. (B) Numbers of nodules formed on the lungs were counted manually ($^{+/+}$, n = 9; $^{-/-}$, n = 6; **P < 0.01). (C) Size of tumors formed by s.c. inoculated melanoma cells at day 21 [$^{+/+}$, n = 8; $^{-/-}$, n = 6; *P > 0.05 (not significant)]. (D) Metastasis of i.v. injected B16F10-luc-G5 cells measured by luminescence using IVIS in vivo imaging at day 7. (E) Quantification of photon counts in C ($^{+/+}$, n = 6; $^{-/-}$, n = 5; *P < 0.05).

which were then injected i.v. into littermates of Stab2$^{+/+}$ and Stab2$^{-/-}$ mice. After 7 d, tumor metastasis was measured based on the luminescence of luciferase. Photon counts were significantly decreased in the Stab2$^{-/-}$ mice, indicating inhibition of metastasis at an early stage (Fig. 2 D and E).

Administration of Anti-Stab2 Antibody Increases Serum HA Levels and Prevents Tumor Metastasis.

We next investigated whether Stab2 functions could be blocked by an anti-Stab2 antibody in vivo. We generated several mAbs against the extracellular domain of Stab2 by immunizing rats with BaF3 cells expressing Stab2 and one of them (#34-2, ref. 10) was found to inhibit HA binding to Stab2 as assessing by internalization of FITC-labeled HSECs in vitro (Fig. 3A). To test whether that anti-Stab2 mAb has any effect on the plasma HA level in vivo, we injected it i.p. into C57BL/6 mice every 3 d and monitored serum HA levels. Within 3 d of the first injection, serum HA levels were increased in all of the mice given the anti-Stab2 mAb, but not in the mice treated with rat IgG (Fig. 3B). We obtained the same results using SCID mice (Fig. 4 A and J). These findings clearly indicate that the anti-Stab2 mAb effectively increased plasma HA levels by inhibiting Stab2 function in vivo. To examine whether this mAb prevents tumor metastasis, we injected mice with either anti-Stab2 mAb or control rat IgG, followed 2 d later by i.v. injection of B16F10 cells. The anti-Stab2 mAb significantly suppressed metastasis (Fig. 3 C and D). Taken together, these results indicate that the anti-Stab2 mAb elevates circulating HA levels by blocking the clearance of HA in HSECs, and that serum HA levels are inversely correlated with tumor metastasis.

Because the anti-Stab2 mAb elevated plasma HA levels in immune deficient mice, we investigated its effect on spontaneous metastasis by multiple cancer cells in SCID mice. To do so, we transplanted MDA-MB-231-luc-D3H2LN cells (human mammary gland adenocarcinoma cells expressing luciferase) into the abdominal mammary glands of SCID mice. After 21 d, tumor metastasis in the upper body, including the brachial lymph nodes, was evaluated by luminescence analysis. The number of photons derived from metastasized cells in the upper body was significantly reduced in the mice treated with the anti-Stab2 mAb (Fig. 4 A–D). We also transplanted 4T1-LucNeo-1H mouse mammary tumor cells expressing luciferase into the mammary fad pads of

the mice. Starting at 2 d after tumor injection, each animal was given either anti-Stab2 mAb or rat IgG every 3 d. At 3 wk after the start of antibody treatment, metastatic luminescence signals and the numbers of histological lesions in the lung were reduced in the anti-Stab2 mAb-treated mice. Given the lack of significant difference in the size of primary tumors (Fig. 4 E–L), anti-Stab2 mAb can be considered to inhibit spontaneous metastasis.

Examination of Possible Mechanisms for Inhibition of Metastasis.

To investigate the inhibitory mechanism of metastasis observed in the Stab2 KO and anti-Stab2 mAb-treated mice, we first analyzed whether HA affects tumor cells in vitro. We evaluated the effects of a 31-kDa HA (similar in size to HA in circulation; Fig. S1J), on cell proliferation, apoptosis induced by hydrogen peroxide, migration, and invasion into the basal membrane. None of these assays demonstrated any significant effect of HA on tumor cells at various concentrations (Fig. S3 A–E).

Because the proliferation as well as metastasis of tumors is under surveillance by the immune system, and HA has been implicated in the immune system, we examined the immune cells of Stab2 KO mice for any changes. We found no significant differences in fractions of regulatory T cells, NK cells, macrophages, and myeloid-derived suppressor cells in bone marrow, peripheral blood, and spleen in Stab2 KO mice compared with WT mice (Fig. S4A). In addition, we found no alterations in serum levels of TNF-α, IFN-γ, IL-2, IL-4, IL-6 IL-10, and IL-17A (Fig. S4B), or in the activation of macrophages in vivo and sensitivity to i.p. LPS (Figs. S2E and S4C). These results showing no significant alterations in the immune system in Stab2 KO mice suggest that the immune system may not be directly involved in the inhibition of tumor metastasis.

Attachment of Melanoma Cells to the Lungs Is Prevented by an Increase in Plasma HA.

Intravenously injected melanoma cells are thought to roll through the bloodstream and lodge in the lungs, where they proliferate. Our finding that the melanoma cells injected s.c. in Stab2 KO mice formed tumors as large as those seen in their WT littermates (Fig. 2C) suggests that the homing of i.v. injected tumor cells to the lungs might be altered in the mutant mice. To analyze the attachment of melanoma cells to the lung in vivo, we inoculated B16F10-luc-G5 cells i.v. After 6 h, mice were perfused with PBS via the portal vein to remove blood cells from the tissues, and luciferase activity in the lungs was evaluated. The luciferase activity in the lungs was significantly decreased in Stab2 KO mice and in mice treated with the anti-Stab2 mAb compared with WT mice and rat IgG-treated mice (Fig. 5 A and B). These results indicate that tumor metastasis was prevented at an early stage of penetration in the lungs.

Because plasma HA level has been suggested to be involved in the metastasis of melanoma cells, and HA binds to cell surface molecules such as CD44, we investigated whether HA mediates the attachment of tumor cells to tissues. We first tested the binding of melanoma cells to HA by plating B16F10 cells on an HA-coated plate, and found that the cells attached to the plate via HA (Fig. S3F). Adding HA at the concentration found in Stab2 KO mouse sera inhibited the binding of B16F10 to the HA-coated plate. This finding suggests that the increased plasma HA in the mutant mice inhibits metastasis by preventing the attachment of melanoma cells to the lung via HA.

We also investigated whether HA prevents the attachment of B16F10 cells to the lung. Although i.v. injected HA is rapidly cleared from the bloodstream (1), we found that a very high dose of HA administered via the tail vain elevated the serum HA level for several hours (Fig. 5C). Thus, we injected HA at a dose of 20 mg/kg body weight every 8 h for 24 h to increase the plasma HA level, and then transplanted B16F10-luc-G5 cells. At 6 h after B16F10-luc-G5 cell transplantation, luciferase activity in the lungs was significantly reduced, whereas the serum
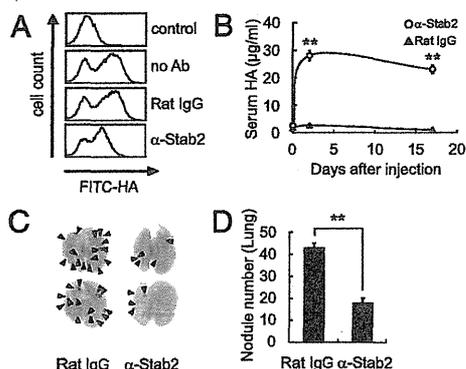

Fig. 3. Inhibition of HA clearance and metastasis by anti-Stab2 mAb. (A) HSECs were incubated with anti-Stab2 mAb or rat IgG, and the cell internalization of FITC-HA was analyzed by flow cytometry. (B) Anti-Stab2 mAb or rat IgG (3 mg/kg body weight) was administered i.p. to C57BL/6 mice on days 0, 3, and 17, and serum HA levels were measured (n = 5; **P < 0.01). (C) At 2 d after the i.p. administration of anti-Stab2 mAb or control IgG, 5 × 10⁴ B16F10 cells were injected i.v. via the tail vein. Anti-Stab2 mAb or control IgG was administered every 3 d. The lungs at 14 d are shown. Arrowheads indicate nodules of B16F10 cells. (D) The number of nodules formed on the lungs were counted manually (n = 10; **P < 0.01). α-Stab2 denotes anti-Stab2 mAb.
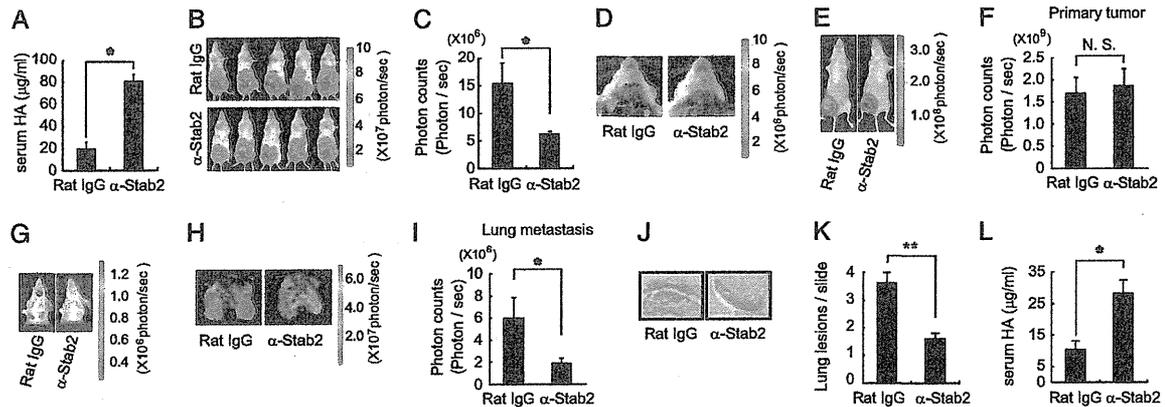
Hirose et al.

Fig. 4. Anti-Stab2 antibody prevents spontaneous metastasis of human and mouse mammary tumor cells in SCID mice. (A) SCID mice were i.p. injected with anti-Stab2 mAb or rat IgG (3 mg/kg), and serum HA levels were measured at 7 d after the injection (n = 5; *P < 0.05). (B) MDA-MB-231-luc-D3H2LN cells were grafted in the mammary gland of SCID mice injected i.p. with anti-Stab2 mAb or control IgG (3 mg/kg). Luminescence was measured by IVIS at day 21. (C) Quantification of photon counts in the upper body at day 21 (n = 5; *P < 0.05). (D) Luminescence of the opened thorax in B. (E) Mouse 4T1-LucNeo-1H mammary tumor cells were grafted into a mammary fat pad of the mice. At 2 d after tumor injection, each animal was given anti-Stab2 mAb or Rat IgG i.p. every 3 d, for a total of seven injections. Luminescence of primary tumors was measured by IVIS at day 21. (G) For the detection of signals from metastatic regions, the lower part of each animal was shielded with black paper before reimaging, to minimize bioluminescence from primary tumor. At the end of the experiment (day 21), ex vivo imaging was performed on collected lungs. Control group mice exhibited spontaneous lung metastasis. (F, H, and I) Quantification of bioluminescence emitted from primary tumors on mice and lung metastatic regions at the end of the experiment. Data represent mean ± SD (n = 4; *P < 0.05 vs. other groups). (J) H&E-stained sections of spontaneous lung metastasis lesions at day 21. (K) Quantification of lung lesions in J. Data represent mean values (n = 32; **P < 0.01 vs. other groups). (L) Serum HA levels measured at the end of the experiment (n = 4; *P < 0.05). α-Stab2 denotes anti-Stab2 mAb.

HA level remained elevated in those mice pretreated with HA (Fig. 5 D and E).

Finally, to prove that increased HA level decreases the arrest of tumor cells in lung capillaries, we performed in vitro rolling/tethering assays using a VenaEC system. Pulmonary ECs from

WT mice were cultured on VenaEC substrates and connected to a microfluidic device. Rolling/tethering between pulmonary cells and B16 melanoma cells under share stress was observed (Fig. 5F). At a low HA concentration (0.55 µg/mL, similar to Stab2^{+/+} serum levels), B16 melanoma cells were tethered to pulmonary
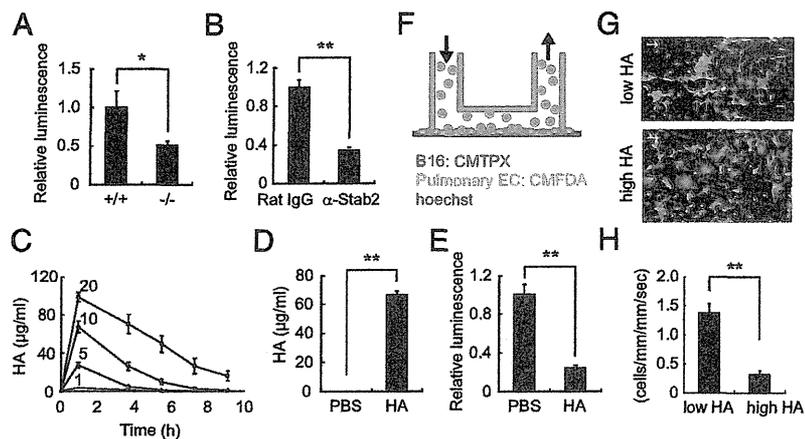

Fig. 5. HA inhibits attachment of B16F10 cells. (A) B16F10-luc-G5 cells (1.5 × 10^6) were injected into the tail vein of Stab2^{+/+} and Stab2^{−/−} mice, and 6 h later, the mice were perfused with PBS via the portal vein to remove blood cells from tissues. The B16F10-luc-G5 cells remaining in the lungs were detected by luciferase analysis (+/+, n = 6; −/−, n = 7; *P < 0.05). (B) At 2 d after the i.p. administration of anti-Stab2 or rat IgG, B16F10-luc-G5 cells (1.5 × 10^6) were injected into the tail vein. At 6 h later, the injection cells remaining in the lungs were detected by luciferase analysis as in A (rat IgG, n = 5; −/−, n = 6; **P < 0.01). (C) HA at doses of 1, 5, 10, and 20 mg/kg was injected i.v., and serum HA levels were measured serially (n = 4). (D) HA at 20 mg/kg or an equal volume of PBS was injected i.v. every 8 h. At 24 h after the first HA injection, B16F10-luc-G5 cells (1.5 × 10^6) were injected into the tail vein with 20 mg/kg of HA. After 6 h, serum samples were collected, and plasma HA levels were analyzed at the end of experiment (n = 8; **P < 0.01). (E) Cells remaining in the lungs were detected based on luciferase activity at D as in A (n = 8; **P < 0.01). (F) Schematic diagram of the VenaEC system (Cellix). (G) Rolling and/or tethering of B16 melanoma cells onto pulmonary ECs using the VenaEC system. Pulmonary ECs from 6-d-old WT (C57BL/6) mice were isolated, cultured, and stained with 5 µM CMFDA (green) and 10 µM Hoechst 33342 (blue). B16F10 cells were stained with 5 µM CMTPX (red) and 10 µM Hoechst (blue). The pulmonary cell chamber was connected to a microfluidic device, and perfusion for 5 min with VL medium containing stained B16F10 cells at 0.7 dynes/cm² was performed during confocal observation of cell kinetics. Representative images of B16 melanoma cells with low (0.55 µg/mL) and high (33 µg/mL) HA concentrations are shown (Movies S1 and S2). White arrows denote flow directions, and red arrows indicate rolling and/or tethering B16F10 cells. (H) Quantification of rolling/tethering to the pulmonary ECs. The numbers of rolling/ tethering B16F10 cells were counted. Note that HA at high concentrations inhibited the rolling/tethering of melanoma cells onto pulmonary endothelium (n = 20 images from five experiments; *P < 0.05). (Scale bar: 100 µm.) α-Stab2 denotes anti-Stab2 mAb.

cells. In contrast, at a high HA concentration (33 μg/mL, similar to Stab2$^{-/-}$ serum levels), tethering was significantly reduced (Fig. 5 G and H and Movies S1 and S2). These results indicate that a high level of HA in the circulation prevents the attachment of melanoma cells to the lung.

Discussion

In this study, using Stab2 KO mice and an anti-Stab2 mAb, we provide several lines of evidence indicating that Stab2 is the major clearance receptor for circulating HA. This finding is consistent with the results of a previous in vitro study showing that Stab2, not its homolog Stab1, is the major clearance receptor for HA (5), as well as a recent study using Stab1 and Stab2 KO mice (2). In addition, KO mice deficient in either Lyve1 or Stab1 showed no change in serum HA levels (2, 29), further supporting this idea. Although Stab2 is known to bind other molecules, such as ac-LDL and heparin, serum levels of ac-LDL and heparin were not increased in the Stab2 KO mice, and the internalization of ac-LDL into Stab2-deficient HSECs was normal, indicating that those molecules are cleared by other scavenger receptors, such as Stab1. Therefore, we conclude that Stab2 is the bona fide clearance receptor for circulating HA in vivo.

An unexpected finding—and perhaps the most important result of this study—is the markedly reduced metastasis of melanoma cells in the Stab2 KO mice. Furthermore, i.p. administration of the blocking mAb for Stab2 also increased the serum concentration of HA and inhibited tumor metastasis in the Stab2$^{+/+}$ mice at levels comparable to those in Stab2 KO mice (Fig. 3). The KO mice were fertile, developed normally, and exhibited no hematological or histological changes except for the increased serum HA level (Fig. S1 and Table S1). Although Stab2 has multiple ligands, only HA levels were altered in the Stab2 KO mice, and the anti-Stab2 mAb caused phenotypes similar to those in the Stab2 KO mice. Thus, we focused on HA to investigate the mechanism preventing metastasis, and carried out various experiments in vitro and in vivo. Our in vitro experiments indicated that HA did not affect the proliferation, migration, and invasion of B16F10 cells (Fig. S3 A–E). Moreover, the weights of tumors formed by s.c. transplanted melanoma cells, as well as the cell cycle status of i.v. injected melanoma cells, were not changed in the Stab2 KO mice, indicating that the lack of Stab2 does not affect tumor proliferation in vivo (Fig. 2C and Fig. S3B). Likewise, mammary tumor cells formed primary tumors in abdominal fat pads, but tumor formation in the lymph nodes or lung was severely suppressed by anti-Stab2 mAb (Fig. 4). These results strongly suggest that tumor metastasis is prevented by a mechanism other than proliferation.

Tumorigenesis is controlled by the immune system, and the role of HA in the immune system has been studied extensively. Of note, HA binds to TLR2 and TLR4, which play important roles in innate immunity (18). We examined several parameters of the immune system, focusing first on macrophage functions, given that HA has been shown to alter immune responses via TLR4 that binds to LPS (18). However, macrophage activation and the severity of sepsis induced by i.p. injected LPS were not changed in Stab2 KO mice or in mice treated with the anti-Stab2 mAb (Figs. S2E and S4C). Furthermore, levels of inflammatory cytokines in serum and populations of various immune cells were not affected (Fig. S4 A and B). Therefore, inhibition of Stab2 function does not appear to directly affect the immune system. It is known that HA's functions depend on its molecular size, which varies from a few kDa to a few MDa (16). In the present study, HA molecules in Stab2 KO serum were ~40 kDa in size (Fig. S1J), possibly explaining some of the discrepancy between our results and those of previous studies.

Tumor cells circulate through the bloodstream and penetrate preferable tissues. Given that the s.c. proliferation of melanoma cells in Stab2 KO mice was not altered (Fig. 2C), we examined the initial step of attachment to the lungs. Melanoma cells expressing luciferase were injected via the tail vein, and cells trapped in the lungs were detected based on luciferase activity after perfusion with PBS to remove nonadherent cells. At 6 h after the i.v. injection, the number of melanoma cells trapped in the lungs was decreased in both the Stab2 KO mice and the mice given anti-Stab2, indicating that tumor metastasis is prevented at the initial stage of tissue penetration in the absence of Stab2 function (Fig. 5 A and B). Because those mice had extremely high plasma HA levels, we considered that the attachment of melanoma cells to the lungs is enhanced by HA displayed on the surface of blood vessels in normal lungs, and that a high level of HA in plasma blocks this interaction. In fact, melanoma cells adhered to HA-coated plates and pulmonary ECs, and HA at high concentrations, similar to those in serum of Stab2 KO mice, inhibited the attachment (Fig. 5, Fig. S3F, and Movies S1 and S2). Although i.v. injected HA is rapidly removed from the circulation, we found that the i.v. injection of a very high dose of HA was able to maintain the plasma HA concentration at a high level for at least 10 h (Fig. 5C). After the circulating HA level increased, B16F10 cells were injected to evaluate their attachment to the lungs. Metastasis of B16F10 cells to the lungs was markedly suppressed under these conditions (Fig. 3D). These results strongly suggest that inhibition of Stab2 function prevents tumor metastasis by elevating the plasma HA level.

Previous studies found that forced expression of HAS increased tumor cell proliferation and metastasis, whereas inhibition of HAS prevented proliferation and metastasis (23, 24, 30). These experiments suggested that HA promotes tumor proliferation and metastasis, whereas our results indicate that HA prevents metastasis. The critical difference between the previous studies and the present study is that we focused on the circulating HA, whereas most of the previous studies investigated extracellular matrix and pericellular HA. Therefore, it seems that the function of HA can differ depending on location.

In conclusion, our Stab2 KO mice were viable and exhibited no overt defects, but had dramatically increased plasma HA levels. This indicates that Stab2 is dispensable for normal development and homeostasis, and that an extremely high level of plasma HA has no deleterious effect. The increase in circulating HA levels was inversely correlated with metastasis and inhibited the attachment of melanoma cells to the lungs. Moreover, the administration of an anti-Stab2 mAb also increased the plasma HA level and blocked the metastasis of not only mouse melanoma cells, but also human breast tumor cells with no side effects. Thus, functional inhibition of Stab2 may be a potential strategy to suppress tumor metastasis.

Materials and Methods

A Stab2 KO mouse line was generated by conventional methods, as described in *SI Materials and Methods*, and backcrossed with C57BL/6 for at least six generations. Anti-mouse Stab2 mAb (#34-2) was generated in our laboratory (10). Serum HA levels were measured with an HA assay kit (Seikagaku Biobusiness) in accordance with the manufacturer's instructions. The cell internalization of FITC-HA into HSECs was performed as described previously (10). For FACS analysis, HSECs were incubated with indicated antibodies and FITC-HA, and labeled cells were analyzed with a FACSCalibur flow cytometer (BD Biosciences). B16F10 cells [5 × 10^5 (Fig. 2) or 5 × 10^4 (Fig. 3)] were injected into the tail vein. At 14 d after injection, the lung surface nodules were counted. For imaging in vivo, 5 × 10^5 B16F10-luc-G5 cells were injected i.v. At 7 d after the injection, metastasis was analyzed with luciferase luminescence as described previously (31). MDA-MB-231-luc-D3H2LN cells (4 × 10^6) were injected into the mammary gland of SCID mice, and metastasis was analyzed using the IVIS imaging system (31, 32). 4T1-LucNeo-1H cells (5 × 10^4) were injected into a mammary fad pad of SCID mice. Rolling and/or tethering of B16 melanoma cells onto cultured pulmonary ECs was analyzed under flow conditions at 0.7 dynes/cm² with the VenaEC System (Cellix) using confocal microscopy (Nikon A1R). Before the experiments, B16 melanoma cells were stained by CellTracker Red CMTPX (Molecular Probes) and Hoechst 33342 (Molecular Probes). Pulmonary ECs were also stained with Cell-Tracker Green CMFDA (Molecular Probes) and Hoechst 33342. More detailed information is provided in *SI Materials and Methods*.

1. Fraser JR, Alcorn D, Laurent TC, Robinson AD, Ryan GB (1985) Uptake of circulating hyaluronic acid by the rat liver: Cellular localization in situ. *Cell Tissue Res* 242: 505–510.
2. Schledzewski K, et al. (2011) Deficiency of liver sinusoidal scavenger receptors stabilin-1 and -2 in mice causes glomerulofibrotic nephropathy via impaired hepatic clearance of noxious blood factors. *J Clin Invest* 121:703–714.
3. Politz O, et al. (2002) Stabilin-1 and -2 constitute a novel family of fasciclin-like hyaluronan receptor homologues. *Biochem J* 362:155–164.
4. Adachi H, Tsujimoto M (2002) FEEL-1, a novel scavenger receptor with in vitro bacteria-binding and angiogenesis-modulating activities. *J Biol Chem* 277:34264–34270.
5. Hansen B, et al. (2005) Stabilin-1 and stabilin-2 are both directed into the early endocytic pathway in hepatic sinusoidal endothelium via interactions with clathrin/AP-2, independent of ligand binding. *Exp Cell Res* 303:160–173.
6. Kzhyshkowska J, et al. (2005) Phosphatidylinositide 3-kinase activity is required for stabilin-1-mediated endosomal transport of acLDL. *Immunobiology* 210:161–173.
7. Kzhyshkowska J, et al. (2008) Alternatively activated macrophages regulate extracellular levels of the hormone placental lactogen via receptor-mediated uptake and transcytosis. *J Immunol* 180:3028–3037.
8. Kzhyshkowska J, et al. (2006) Novel function of alternatively activated macrophages: Stabilin-1-mediated clearance of SPARC. *J Immunol* 176:5825–5832.
9. Salmi M, Koskinen K, Henttinen T, Elima K, Jalkanen S (2004) CLEVER-1 mediates lymphocyte transmigration through vascular and lymphatic endothelium. *Blood* 104: 3849–3857.
10. Nonaka H, Tanaka M, Suzuki K, Miyajima A (2007) Development of murine hepatic sinusoidal endothelial cells characterized by the expression of hyaluronan receptors. *Dev Dyn* 236:2258–2267.
11. Park SY, et al. (2008) Rapid cell corpse clearance by stabilin-2, a membrane phosphatidylserine receptor. *Cell Death Differ* 15:192–201.
12. Gustafson S, Björkman T (1997) Circulating hyaluronan, chondroitin sulphate and dextran sulphate bind to a liver receptor that does not recognize heparin. *Glycoconj J* 14:561–568.
13. Harris EN, Weigel PH (2008) The ligand-binding profile of HARE: Hyaluronan and chondroitin sulfates A, C, and D bind to overlapping sites distinct from the sites for heparin, acetylated low-density lipoprotein, dermatan sulfate and CS-E. *Glycobiology* 18:638–648.
14. Kogan G, Soltés L, Stern R, Gemeiner P (2007) Hyaluronic acid: A natural biopolymer with a broad range of biomedical and industrial applications. *Biotechnol Lett* 29: 17–25.
15. Fraser JR, Laurent TC, Laurent UB (1997) Hyaluronan: Its nature, distribution, functions and turnover. *J Intern Med* 242:27–33.
16. Stern R, Asari AA, Sugahara KN (2006) Hyaluronan fragments: An information-rich system. *Eur J Cell Biol* 85:699–715.
17. Almond A (2007) Hyaluronan. *Cell Mol Life Sci* 64:1591–1596.
18. Jiang D, et al. (2005) Regulation of lung injury and repair by Toll-like receptors and hyaluronan. *Nat Med* 11:1173–1179.
19. DeGrendele HC, Estess P, Siegelman MH (1997) Requirement for CD44 in activated T cell extravasation into an inflammatory site. *Science* 278:672–675.
20. Zöller M (2011) CD44: Can a cancer-initiating cell profit from an abundantly expressed molecule? *Nat Rev Cancer* 11:254–267.
21. Banerji S, et al. (1999) LYVE-1, a new homologue of the CD44 glycoprotein, is a lymph-specific receptor for hyaluronan. *J Cell Biol* 144:789–801.
22. Kim S, et al. (2009) Carcinoma-produced factors activate myeloid cells through TLR2 to stimulate metastasis. *Nature* 457:102–106.
23. Sironen RK, et al. (2011) Hyaluronan in human malignancies. *Exp Cell Res* 317: 383–391.
24. Toole BP (2004) Hyaluronan: From extracellular glue to pericellular cue. *Nat Rev Cancer* 4:528–539.
25. Twarock S, et al. (2011) Inhibition of oesophageal squamous cell carcinoma progression by in vivo targeting of hyaluronan synthesis. *Mol Cancer* 10:30.
26. Kudo D, et al. (2004) Effect of a hyaluronan synthase suppressor, 4-methylumbelliferone, on B16F-10 melanoma cell adhesion and locomotion. *Biochem Biophys Res Commun* 321:783–787.
27. Zhou B, Weigel JA, Fauss L, Weigel PH (2000) Identification of the hyaluronan receptor for endocytosis (HARE). *J Biol Chem* 275:37733–37741.
28. Harris EN, Weigel JA, Weigel PH (2008) The human hyaluronan receptor for endocytosis (HARE/Stab2) is a systemic clearance receptor for heparin. *J Biol Chem* 283: 21453–21461.
29. Gale NW, et al. (2007) Normal lymphatic development and function in mice deficient for the lymphatic hyaluronan receptor LYVE-1. *Mol Cell Biol* 27:595–604.
30. Yoshihara S, et al. (2005) A hyaluronan synthase suppressor, 4-methylumbelliferone, inhibits liver metastasis of melanoma cells. *FEBS Lett* 579:2722–2726.
31. Takeshita F, et al. (2005) Efficient delivery of small interfering RNA to bone-metastatic tumors by using atelocollagen in vivo. *Proc Natl Acad Sci USA* 102:12177–12182.
32. Jenkins DE, Hornig YS, Oei Y, Dusich J, Purchio T (2005) Bioluminescent human breast cancer cell lines that permit rapid and sensitive in vivo detection of mammary tumors and multiple metastases in immune deficient mice. *Breast Cancer Res* 7:R444–R454.

Micromanaging Iron Homeostasis

HYPOXIA-INDUCIBLE MICRO-RNA-210 SUPPRESSES IRON HOMEOSTASIS-RELATED PROTEINS*[S]

Yusuke Yoshioka[‡§1], Nobuyoshi Kosaka[§], Takahiro Ochiya[§], and Takashi Kato[‡¶2]

From the ‡Integrative Bioscience and Biomedical Engineering, Graduate School of Science and Engineering, Waseda University, 2-2 Wakamatsu, Shinjuku, Tokyo 162-8480, Japan, the §Translational Research Group Division of Molecular and Cellular Medicine, National Cancer Center Research Institute, 5-1-1 Tsukiji, Chuo-ku, Tokyo 104-0045, Japan, and the ¶Department of Biology, School of Education, Waseda University, Tokyo 162-8480, Japan

Background: The regulatory mechanisms of iron homeostasis in cancer cells are not yet fully understood.

Results: MicroRNA-210 suppresses two essential molecules for iron homeostasis, TfR and ISCU.

Conclusion: Precise regulation of microRNA-210 expression level is vital for maintaining the iron homeostasis, leading to the survival of cancer cells.

Significance: This study reveals the linkages among hypoxia, iron homeostasis, and cancer.

Iron is fundamental for sustaining life for living organisms, and the iron metabolism is finely regulated at different levels. In cancer cells, deregulation of the iron metabolism induces oxidative stress and drives tumor progression and metastasis; however, the molecular mechanisms of iron homeostasis are not fully understood. Here we found that iron deficiency as well as hypoxia promoted microRNA-210 (miR-210) expression. A central mediator of miR-210 transcriptional activation is the hypoxia-inducible factor (HIF)-1α, and the hypoxia-response element in the miR-210 promoter is confirmed experimentally. This is in agreement with the data from in vivo studies that have demonstrated the presence of miR-210-expressing cells at the chronic hypoxic regions of xenografted tumors. Furthermore we found two essential molecules for iron homeostasis, iron-sulfur cluster scaffold protein (ISCU) and transferrin receptor 1 (TfR), are a direct target of miR-210. Transfection of miR-210 decreases the uptake of transferrin by inhibiting the expression of TfR. In addition, inhibition of miR-210 by anti-miR-210 up-regulates ISCU expression. These findings suggest that miR-210 works as an iron sensor and is involved in the maintenance of iron homeostasis by sustaining the TfR expression level to stimulate cell proliferation and promote cell survival in the hypoxic region within tumors.

During the evolutionary processes, life has made use of iron in a variety of biochemical processes. For instance, iron is an essential cofactor for nonheme enzymes, such as ribonucleotide reductase, which is essential for DNA synthesis and is also a vital component of the heme in the oxygen-binding protein, hemoglobin (1–3). Iron needs to be tightly regulated, as excess iron is toxic and causes the generation of free radicals (4), whereas iron insufficiency induces hypoferric anemia in mammals (5) coupled to hypoxia in tissues (6, 7). Given the links between iron metabolism and oxygen transport, the associations between the control of the iron concentration and the physiology of the hypoxic response are important (8). Many responses to altered oxygen levels are coordinated by a hypoxia-inducible factor (HIF)[3] (9, 10).

The association between iron and cancer has been shown in animal models and epidemiologic studies in several human cancers. For instance, the oldest reported experiment of iron-induced carcinogenesis is that of mice exposed to iron-oxide dust, which caused pulmonary tumors (11). In addition, various studies have also shown higher levels of expression of the transferrin receptor 1 (TfR), which is an essential protein involved in iron uptake and the regulation of cell growth, in cancer cells than in their normal counterparts (12). TfR could be attributed to the increased need for iron as a cofactor of ribonucleotide reductase involved in the DNA synthesis of rapidly dividing cells. These reports suggest that iron homeostasis is important in cancer initiation and progression. However, the regulatory mechanisms of iron homeostasis in cancer cells are not yet fully understood.

MicroRNAs (miRNAs) have emerged as a new class of noncoding genes involved in regulating a wide variety of biological processes (13, 14), and their mis-expression has been shown to contribute to tumorigenesis (15). Therefore, miRNAs act as

tuners of gene expression and maintain homeostasis. For instance, miR-144/451 knockout mice display a cell autonomous impairment of late erythroblast maturation, resulting in erythroid hyperplasia, splenomegaly, and mild anemia (16).

In a previous report, we demonstrated that miR-210 is highly expressed in human and murine erythroid cells and in the spleen of mice with hemolytic anemia (17). Erythrocytes require iron to perform their duty as oxygen carriers. Recent reports have shown that the expression of miR-210 is induced by hypoxic conditions (18). Therefore, miR-210 might play an important role in the connection of iron and oxygen. It was already reported that the expression of miR-210 was tightly associated with poor prognosis of breast cancer (18); however, contradictory data exist concerning the regulation and roles of miR-210 during cancer progression. In this study, we clarified that miR-210 regulates iron homeostasis in cancer cells. The expression of miR-210 was induced not only in hypoxic conditions but also in iron deficiency. In addition, we found that the targets of miR-210 are two essential molecules for iron homeostasis, TfR and the iron-sulfur cluster scaffold protein (ISCU). Furthermore, we showed that the distribution of miR-210-expressing cells in inoculated tumor cells could be observed in the chronic hypoxic regions. These results indicated that iron-deficiency-inducible miR-210 controls the expression of two iron regulatory proteins to optimize the survival and proliferation rate of cancer cells located in the chronic hypoxic regions.

EXPERIMENTAL PROCEDURES

Reagents—Rabbit polyclonal anti-ISCU (FL-142) (sc-28860) was purchased from Santa Cruz Biotechnology (Santa Cruz, CA). Mouse monoclonal anti-TfR (13-6800) was purchased from Invitrogen. Mouse monoclonal anti-actin, clone C4 (MAB1501), was purchased from Millipore (Billerica, MA). Mouse monoclonal anti-HIF-1α (610959) was purchased from BD Biosciences. Rabbit monoclonal anti-ferritin (EPR3004Y) was purchased from Epitomics (Burlingame, CA). Rabbit polyclonal anti-ACO1/iron regulatory protein 1 (IRP1) was purchased from Medical & Biological Laboratories Co., Ltd. Rabbit polyclonal anti-red fluorescent protein (ab34771) was purchased from Abcam (Cambridge, MA). Peroxidase-labeled anti-mouse and anti-rabbit antibodies were included in the Amersham Biosciences ECL Plus Western blotting reagents pack (RPN2124) (GE Healthcare). Synthetic hsa-miR-210 (pre-miR-210) and antisense miR-210 oligonucleotide (anti-miR-210) were purchased from Ambion (Austin, TX). The duplexes of each small interfering RNA (siRNA) targeting human HIF-1α mRNA (s30925; target sequences of 5'-GGAGGU-GUUUGACAAGCGAdTdT-3' and 5'-UCGCUUGUCAAA-CACCUCCtg-3'), an siRNA-specific for human IRP1 (ACO1) mRNA (target sequences of 5'-GCUCGCUACUUAACUAA-CAtt-3' and 5'-UGUUAGUUAAGUAGCGAGCag-3') and negative control 1 (NC1) were purchased from Applied Biosystems. An siRNA-specific for human TfR mRNA (target sequences of 5'-GAACCUGGAUAAUGAUGAAdTdT-3' and 5'-UUCAUCAUUAUCCAGGUUCdTdT-3') was purchased from Sigma-Genosys. Desferrioxamine (DFO) was purchased from Calbiochem. Geneticin was purchased from Invitrogen.

Cell Culture—MCF7 cells and MD-MB-231-luc-D3H2LN cells (Xenogen), a human breast cancer cell line, were cultured in RPMI 1640 medium containing 10% heat-inactivated fetal bovine serum (FBS) and an antibiotic-antimycotic (Invitrogen) at 37 °C in 5% CO_2.

Exposure to Hypoxia—Cells were exposed for 24 h or 48 h either to standard nonhypoxic cell culture conditions (20% O_2, 5% CO_2 at 37 °C) or to hypoxia (1% O_2, 5% CO_2 with N_2 balance at 37 °C) in either a modular hypoxia chamber (Wakenyaku) or a tissue culture incubator.

RNA Extraction—RNA was isolated using TRIzol (Invitrogen) and processed according to the manufacturer's instructions.

Quantitative Real-time RT-PCR (qRT-PCR)—Hsa-miR-210 and endogenous control RNU6B TaqMan qRT-PCR kits and human-ISCU, human-TfR, and human-β-actin TaqMan Gene Expression Assays were purchased from Applied Biosystems (Foster City, CA). The reverse transcription and TaqMan quantitative PCR were performed according to the manufacturer's instructions. PCR was carried out in 96-well plates using the 7300 Real-Time PCR System (Applied Biosystems). All reactions were done in triplicate.

The expression levels of pri-miR-210 and β-actin were measured by qRT-PCR using a SYBR Green PCR Master Mix (Invitrogen). Primer sequences are as follows (shown 5' to 3'): pri-miRNA-210_F, GACTGGCCTTTGGAAGCTCC and R, ACAGCCTTTCTCAGGTGCAG; β-actin_F, GGCACCAC-CATGTACCCTG and R, CACGGAGTACTTGCGCTCAG.

In Silico MicroRNA Target Prediction—Bioinformatic prediction of target genes and miRNA-binding sites was performed using three programs: TargetScan (version 5.0) (19), Sanger miRBase (version 5) (20), and MirTarget2 (21).

3'-UTR Assay Plasmid Constructs—A 297-bp fragment from the 3'-UTR of ISCU containing the predicted target sequence of miR-210 (located at positions 102–109 of the ISCU1/2 3'-UTR) and a 385-bp fragment from the 3'-UTR of TfR containing the predicted target sequence of miR-210 (located at positions 229–235 of this fragment) were PCR-cloned from MCF7-isolated total RNA. Three prime A-overhang was added to the PCR products after 15 min of regular *Taq* polymerase treatment at 72 °C. The PCR products were cloned into a pGEM-T Easy Vector (Promega; Madison, WI). A pair of primers including XhoI and NotI restriction sites was designed to amplify the 3'-UTR of ISCU and TfR insert. The amplified products were ligated into the XhoI and NotI sites of the 3'-UTR of the *Renilla* luciferase gene in the psi-check-2 plasmid (Promega) to generate psi-ISCU and psi-TfR. Primer sequences are as follows (shown 5' to 3'): ISCU_F, GCTCGA-GTAACTCCGTTACTTCCAGCAGGC and ISCU_R, GCGG-CCGCTAATATGCACTTCACGGGCTATC; TfR_F, GCTC-GAGTAATCAGCTGTTTGTCATAGGGC and TfR_R, GCG-GCCGCTAGGTCATGCACGATTGTCCGA. Site-directed mutagenesis or deletion mutant was performed in the seed sequences of ISCU and TfR. PrimeStar Max DNA Polymerase (Takara; Kyoto, Japan) was used for PCR amplification. Forward primer and reverse primer sequences are as follows (shown 5' to 3'): ISCU_mut_F, AGATGTATGTGGTACTTG-CTGTTCACGTTA and ISCU_mut_R, GTACCACATACAT-

CTCATAGCTCTTCGGT; ISCU_del_F, ATGAGATTACTT-
GCTGTTCACGTTA and ISCU_del_R, GCAAGTAATCTC-
ATAGCTCTTCGGT; TfR_mut_F, TGTTGCACGCGCGTA-
CTTAAATGAAAGCA and TfR_mut_R, TACGCGCGTGCA-
ACACCCGAACCAGGAAT; TfR_del_F, CGGGTGTTCGT-
ACTTAAATGAAAGCA and TfR_del_R, AAGTACGAACA-
CCCGAACCAGGAAT.

Immunoblot Analysis—SDS-PAGE gels were calibrated with Precision Plus Protein standards (161-0375) (Bio-Rad), and anti-HIF-1α (1:500), anti-ISCU (1:200), anti-TfR (1:500), and anti-actin (1:1000) were used as primary antibodies. The dilution ratio of each antibody is indicated in parentheses. Two secondary antibodies (peroxidase-labeled anti-mouse and anti-rabbit antibodies) were each used at a dilution of 1:10,000. Bound antibodies were visualized by chemiluminescence using the ECL Plus Western blotting detection system (RPN2132) (GE Healthcare), and luminescent images were analyzed with a LuminoImager (LAS-3000; Fuji Film Inc.).

Flow Cytometric Analysis—MCF7 cells and MDA-MB-231-luc-D3H2LN cells were transfected with pre-miR-210 or pre-NC. After culturing for 48 h, transfected cells were serum-starved for 30 min and then incubated for 45 min in a serum-free medium containing 50 μg of transferrin/ml conjugated with Alexa Fluor 594 (Invitrogen). Transfected cells were suspended in their culture medium and subjected to a FACSAria II cell sorter (BD Biosciences). At least one million cells were pelleted by centrifugation at 180 $\times$ g for 5 min at 4 °C, resuspended in a 20 μl of a monoclonal mouse anti-human CD71-FITC antibody (BD Biosciences, clone M-A712), and incubated for 30 min at 4 °C. Three independent experiments were performed.

Transferrin-uptake Analysis—Transferrin-uptake experiments were performed 48 h after transfection with pre-miR-210 or pre-NC. Transfected cells were serum-starved for 30 min and then incubated for 45 min in a serum-free medium containing 50 μg of transferrin/ml conjugated with Alexa Fluor 594. Cells were then washed and fixed in 4% paraformaldehyde for 15 min at room temperature. After washing with PBS, they were incubated with mouse anti-TfR antibody diluted 1:100 in Dako REAL Antibody Diluent (Dako; Carpinteria, CA) for 1 h. They were then incubated with Alexa Fluor 488 goat anti-mouse IgG diluted 1:1000 in Dako REAL Antibody Diluent for 45 min. Finally, the cells were stained with the fluorescent DNA-binding dye Hoechst 33342 (Invitrogen) for 5 min.

Establishment of Stable Cell Lines—Stable knockdown of ISCU MCF7 cell lines was generated by selection with 4 μg/ml blasticidine (Invitrogen). MCF7 cells were transfected with 0.5 mg of an siISCU1/2 vector or a negative control vector at 90% confluence in 24-well dishes using a Lipofectamine LTX reagent in accordance with the manufacturer's instructions. After 24 h, the cells were replated in a 10-cm dish followed by 3-week selection with 4 μg/ml blasticidine.

Immunohistochemical Staining—Between all consecutive steps of the staining procedure, the sections were rinsed three times for 5 min in PBS. The sections were first fixed in 10% formalin for 4 h. After re-hydration of the tissue sections in PBS for 1 h, they were incubated with mouse anti-HIF-1α diluted 1:500 and rabbit anti-red fluorescent protein diluted 1:100 in Dako REAL Antibody Diluent for 1 h. Sections were then incu-

bated with Alexa Fluor 488 goat anti-mouse IgG and Alexa Fluor 594 goat anti-rabbit IgG (Molecular Probes; Leiden, The Netherlands) diluted 1:1000 in Dako REAL Antibody Diluent for 45 min. Finally, sections were mounted on ProLong Gold antifade reagent with DAPI (Invitrogen).

In Vivo miR-210-monitoring Assay—The pDsRed-Express-DR vector (Clontech Laboratories), which is a promoterless vector that encodes DsRed-Express-DR, was purchased from Takara Bio. This protein is a destabilized variant of the red fluorescent protein. For miR-210 promoter-driven fluorescent-based reporter assays, pmiR-210-DsRed was constructed by inserting a miR-210 promoter region into a multi-cloning site of pDsRed-Express-DR vector at HindIII and XhoI sites. A sensor vector for miR-210 was constructed by introducing tandem binding sites with a perfect complementarity sequence to miR-210, separated by a four-nucleotide spacer into the NotI site of pDsRed-Express-DR vector, which already introduced the CMV promoter into the multi-cloning site. The sequences of the binding site are as follows: 5'-AGTGATTCAGCCGCTG-TCAC*ACGCACA*GACGCGTTCAGCCGCTGTCAC*ACGC-ACA*GATCGAA-3' (sense) and 5'-TTCGATC*TGTGCGTG*-TGACAGCGGCTGAACGCGTC*TGTGCGTG*TGACAGC-GGCTGAATCACT-3' (antisense). The seed sequence of miR-210 is indicated in bold italics. All plasmids were verified by DNA sequencing.

Statistical Analysis—Data presented as *bar graphs* are the means $\pm$ S.E. of at least three independent experiments. Statistical analysis was performed using Student's *t* test.

RESULTS

Iron Deficiency Induces the Expression of miR-210 through the HIF-1α, and miR-210 Directly Suppresses ISCU—To try to determine the possible contribution of miR-210 in the regulation of iron homeostasis, we first measured the expression of miR-210 in breast cancer cells, MCF7 and MDA-MB-231 (MM231) cells, and human breast epithelial cells, MCF10A, after treatment with an iron chelator, DFO. The expression level of miR-210 was increased 3–5-fold above basal levels by the 48 h of DFO treatment compared with untreated cells (Fig. 1*A*). In addition, excess amounts of iron by addition of 500 mM ferric ammonium citrate had no effect on the induction or suppression of the expression of miR-210. To further analyze whether the biogenesis of miR-210 during iron depletion is regulated by a transcriptional mechanism or processing machinery of miRNA biogenesis, we quantified the expression of primary miR-210 (pri-miR-210) in MCF7 cells. The expression of pri-miR-210 levels was induced 1.5–3.5-fold above basal levels by the DFO treatment compared with untreated cells (Fig. 1*B*). This result indicated that the induction of miR-210 is because of transcriptional regulation. As shown previously, the transcription of miR-210 was regulated by iron-deficient-induced HIF-1α through the binding of hypoxia-responsible elements that are located upstream of the miR-210 gene (22) (supplemental Fig. S1, *A–D*). Indeed, suppression of HIF-1α by siRNA (supplemental Fig. S1*E*) leads to a significant reduction of miR-210 expression after treatment with DFO (Fig. 1*C*).

Recent reports showed that miRNAs play a role in feedback and feed-forward transcriptional regulation (23, 24). Previ-
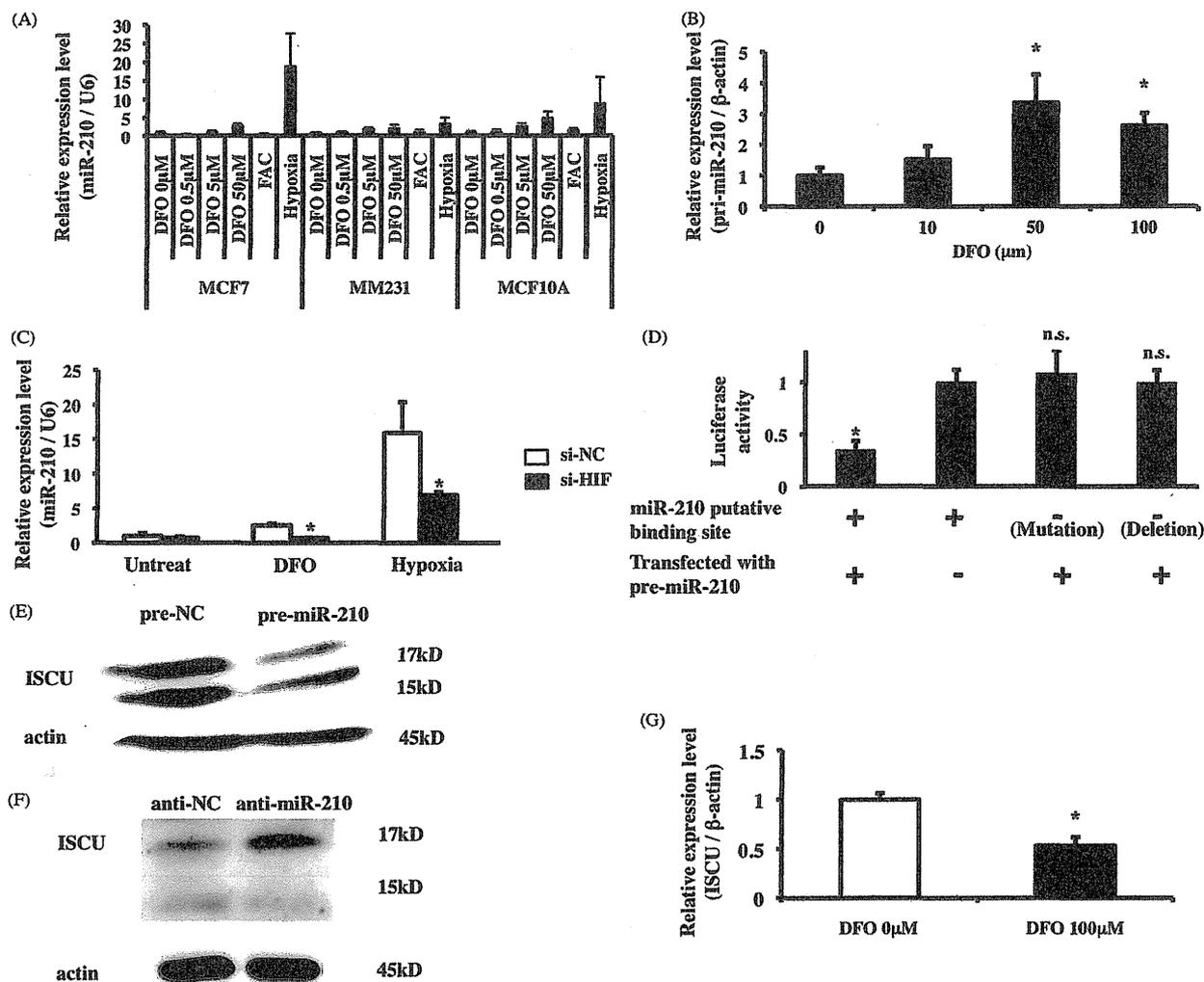
FIGURE 1. **Expression of miR-210 is induced by iron deficiency, and target gene of miR-210 is ISCU.** *A,* miR-210 expression was detected by qRT-PCR after treatment with various concentrations of DFO or exposure to 1% O_2 for 48 h. RNU6B was used as a control. *B,* primary miR-210 expression was detected by qRT-PCR after treatment with DFO for 48 h. β-Actin was used as a control. *C,* MCF7 cells were transfected with HIF-1α siRNA or control siRNA and treatment with DFO 50 μM or exposure to 1% O_2 for 24 h. miR-210 expression was detected by qRT-PCR. RNU6B was used as a control. *, $p < 0.05$ compared with control siRNA groups. *D,* MCF7 cells were co-transfected with pre-miR-210 or pre-NC and psi-ISCU or with its mutant or deletion vector. After 48 h, luciferase activities were measured. *, $p < 0.05$ compared with pre-NC. *n.s.,* not significant. *E,* MCF7 cells were transfected with pre-miR-210 or pre-NC. After 48 h, ISCU expression was detected by immunoblotting. Actin was used as a loading control. *F,* MCF7 cells were transfected with anti-miR-210 or anti-NC and exposed to 1% O_2. After 48 h, ISCU expression was detected by immunoblotting. Actin was used as a loading control. *G,* ISCU expression was detected by qRT-PCR after treatment with DFO 100 μM for 48 h. *, $p < 0.05$ compared with untreated cells. β-Actin was used as a control.

ously, we reported that miR-210 is involved in the production of erythrocytes, which consume 70% of body iron in humans and are the major carriers of oxygen (17, 25). Based on those reports and our finding that the expression of miR-210 was regulated by the iron concentration through the activation of HIF-1α in this study (Fig. 1, *A–C,* and supplemental Fig. S1), we hypothesized that miR-210 regulates genes that are associated with a potent iron homeostasis and a hypoxic cellular response. According to these criteria, ISCU was predicted as a miR-210 target by miRNA target prediction algorithm programs (supplemental Fig. S2A). ISCU is an essential factor of the mitochondria electron transport chain, and loss of function of ISCU can disrupt iron homeostasis (26). Although ISCU was known to be regulated by miR-210 in hypoxic condition (27, 28), the precise mechanism of miR-210 on iron homeostasis in cancer cells has

not been clarified yet. As shown in Fig. 1D, miR-210 recognized the 3'-UTR of ISCU. On the contrary, miR-210 seed sequence in the 3'-UTR of ISCU was mutated or deleted, miR-210 could not bind to the 3'-UTR of ISCU (Fig. 1D). In addition, overexpression or knockdown of miR-210 in MCF7 cells down-regulated or up-regulated the expression of ISCU assessed by qRT-PCR (supplemental Fig. S2, C and D) and immunoblotting (Fig. 1, E and F). These results are consistent with previous findings that ISCU was a direct target of miR-210. To understand the contribution of miR-210 and ISCU on iron homeostasis in breast cancer cells, we checked the expression of ISCU under the condition of iron depletion in breast cancer cells. As shown in Fig. 1G, the expression of ISCU was down-regulated after the treatment with DFO, suggesting that the expression of ISCU was controlled by iron-deficient-induced miR-210 in breast
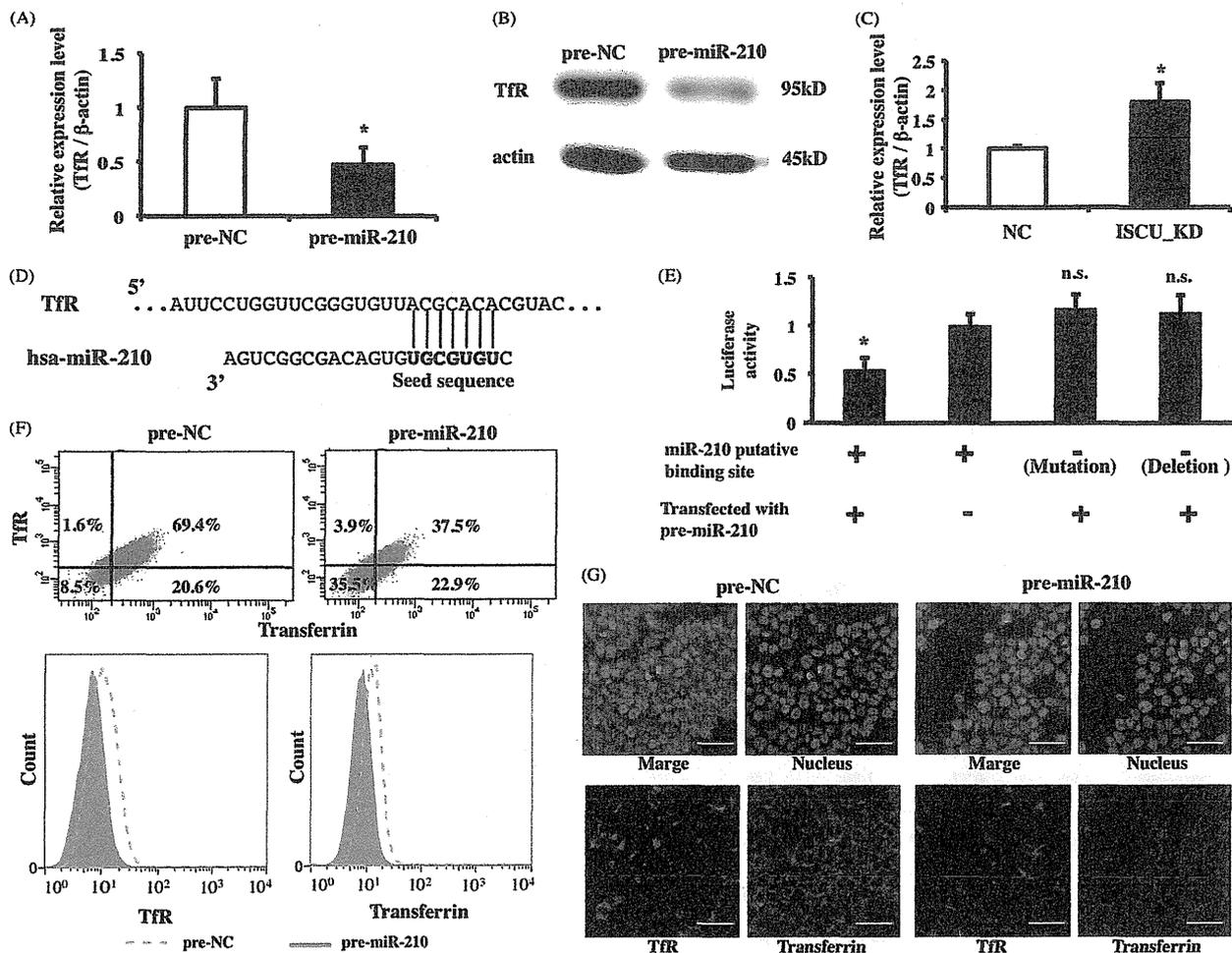
FIGURE 2. miR-210 also represses the expression of TfR as a target gene. *A*, MCF7 cells were transfected with pre-miR-210 or pre-NC. After 48 h, TfR expression was detected by qRT-PCR. β-Actin was used as a control. *, $p < 0.05$ compared with pre-NC. *B*, MCF7 cells were transfected with pre-miR-210 or pre-NC. After 48 h, TfR expression was detected by immunoblotting. Actin was used as a loading control. *C*, expression of TfR is increased by knockdown of ISCU. TfR expression was detected in ISCU knockdown cells by qRT-PCR. β-Actin was used as a control. *ISCU_KD*, ISCU knockdown cell line; *NC*, control cell line. *, $p < 0.05$ compared with the control group. *D*, the predicted binding site for miR-210 at 3′-UTR of TfR gene is shown. The *bold font* shows the seed sequence of miR-210. *E*, MCF7 cells were co-transfected with pre-miR-210 or pre-NC and psi-TfR or with its mutant or deletion vector. After 48 h, luciferase activities were measured. *, $p < 0.05$ compared with pre-NC. *n.s.*, not significant. *F*, MCF7 cells were transfected with pre-miR-210 or pre-NC. After 48 h, transfected cells were incubated with Alexa Fluor 594-labeled Tf for 45 min. Expression of TfR (*y* axis) and uptake of transferrin (*x* axis) (*upper panel*) were analyzed by FACS. The *right lower panel* represents the expression of TfR. The *left lower panel* represents uptake of transferrin. *Dashed histogram*, transfected pre-NC; *filled histogram*, transfected pre-miR-210. *G*, MCF7 cells were transfected with pre-miR-210 or pre-NC. After 48 h, transfected cells were incubated with Alexa Fluor 594-labeled Tf (*red*) for 45 min and fixed in 4% paraformaldehyde for 30 min. Subsequently, cells were immunostained using anti-TfR antibody and an Alexa Fluor 488-conjugated secondary antibody (*green*). The nucleus was then stained with the Hoechst 33342 (*blue*). *Scale bar*, 50 μm.

cancer cells. These results prompted us with the idea that iron-ISCU pathway might regulate the iron homeostasis in breast cancer cells.

miR-210 Suppresses the Major Iron-uptake Protein TfR—In mammalian cells, knockdown of ISCU markedly reduces mitochondrial aconitase activity and then promotes the activity of IRP1. Activation of IRP1 accelerates the binding to multiple iron-responsive elements in the 3′-UTR of the mRNA, such as TfR involved in iron acquisition, then leading to increased mRNA stability (26). When IRP1 binds to the 3′-UTR of TfR mRNA, which is an iron-uptake protein, the transcript is protected from degradation. Therefore, we hypothesized that overexpression of miR-210 stabilizes mRNA of TfR via the activation of IRP1. To prove this hypothesis, we measured the expression of mRNA and the protein level of TfR after transfec-

tion of the miR-210 mimic (pre-miR-210) in MCF7 and MM231 cells. Surprisingly, the expression of TfR was downregulated after the transfection of pre-miR-210 (Fig. 2, *A* and *B*, and supplemental Fig. S4A). This is an unexpected result because the expression of TfR was increased in ISCU stably knockdown cells (Fig. 2C and supplemental Fig. S2E). Those results led us to consider that miR-210 directly suppressed the expression of TfR by binding to the 3′-UTR of TfR. To check whether or not TfR is a direct target gene of miR-210, we once again used *in silico* algorithms and found that there was an miR-210-binding site at 3′-UTR of TfR (Fig. 2D). To prove that miR-210 directly recognizes the identical predicted target site in the 3′-UTR of TfR, MCF7 cells were transfected with psi-TfR, which was fused to 3′-UTR of TfR and the luciferase open reading frame, or a control vector. In addition, we also prepared
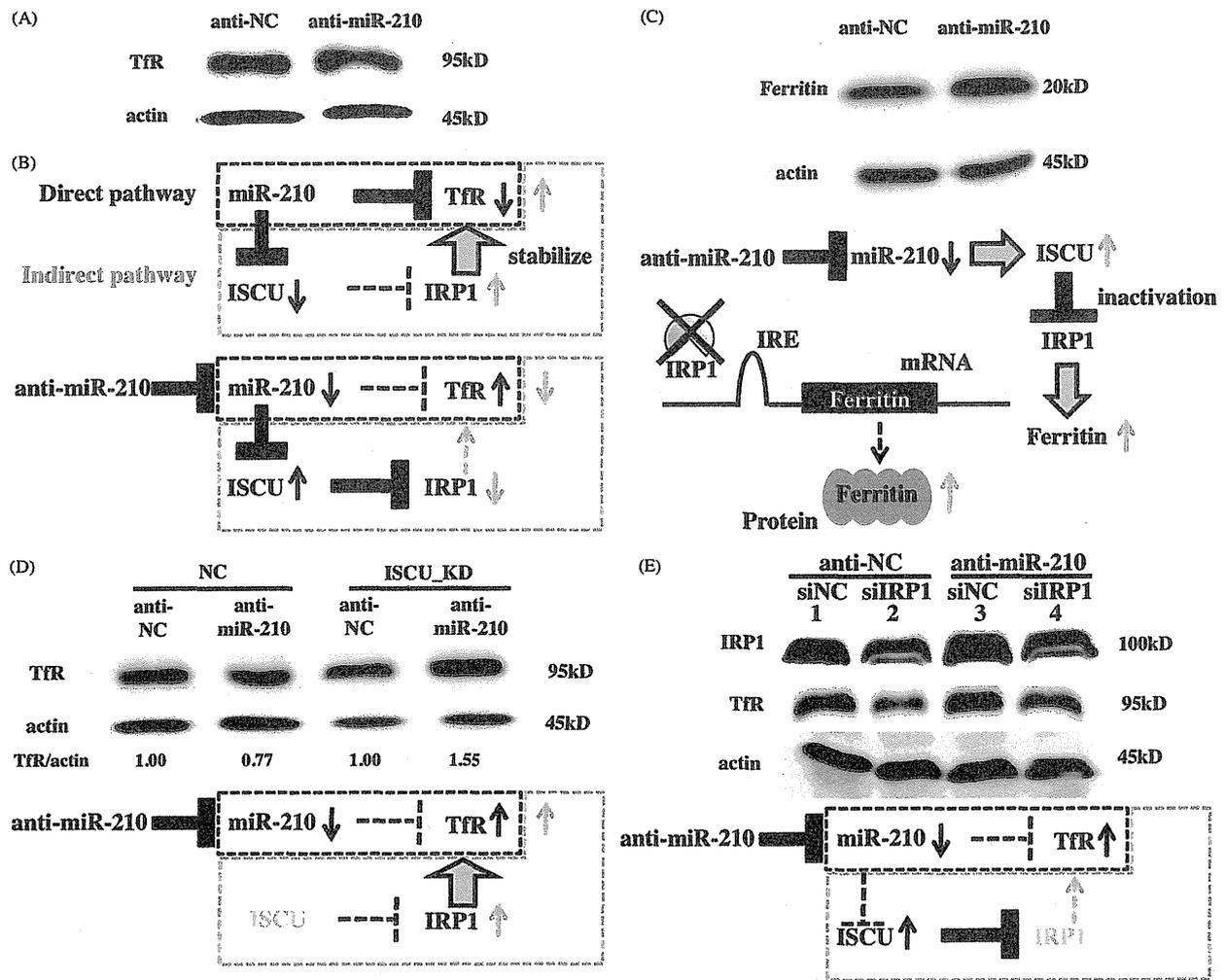
FIGURE 3. **miR-210 has two pathways for regulating TfR expression.** *A,* MCF7 cells were transfected with anti-miR-210 or anti-NC and exposed to 1% O_2 for 48 h. TfR expression was detected by immunoblotting. Actin was used as a loading control. *B,* schematic represents the regulation of two miR-210 target genes after treatment with anti-miR-210. After the transfection of anti-miR-210, the expression of TfR was indirectly decreased via the up-regulation of ISCU. On the other hand, the expression of TfR was directly increased through the down-regulation of miR-210. The expression of TfR then seemed to be unchanged after the transfection of anti-miR-210. *Direct pathway* means that miR-210 recognized the 3′-UTR of TfR and directly (see *black box*) regulates its expression. On the other hand, *Indirect pathway* means that miR-210 indirectly regulates TfR expression through the ISCU-IRP1 pathway (see *gray box*). After the transfection of anti-miR-210 (see *lower panel*), the expression of miR-210 was down-regulated, and then the expression of TfR was up-regulated (see *black box*). On the other hand, expression of ISCU was up-regulated after the transfection of anti-miR-210, and then the activity of IRP1 was inhibited by up-regulation of ISCU. IRP1 was important for the translation of TfR. Thus, inhibition of IRP1 activity by up-regulation of ISCU results in the down-regulation of TfR (see *gray box*). *C,* MCF7 cells were transfected with anti-miR-210 or anti-NC and exposed to 1% O_2. After 48 h, ferritin expression was detected by immunoblotting. Actin was used as a loading control. *Lower panel* shows schematic representation of the regulation of miR-210 target gene and ferritin after treatment with anti-miR-210. *D,* ISCU knockdown cell lines were transfected with anti-miR-210 or anti-NC and exposed to 1% O_2 for 48 h. TfR expression was detected by immunoblotting and quantified by densitometry. Actin was used as a loading control. *Lower panel* shows schematic representation of the regulation of miR-210 target gene after treatment with anti-miR-210 in *ISCU_KD* cells. Because ISCU was stably suppressed by shRNA in these cells, the activity of IRP1 was increased (*gray box*). Therefore, in this experiment, TfR was up-regulated by not only the down-regulation of miR-210 that directly targets the TfR but also the activation by IRP1. *E,* MCF7 cells were transfected with anti-miR-210 or anti-NC and siIRP1 or siNC and exposed to 1% O_2 for 48 h. Expression of IRP1 (*upper*) and TfR (*middle*) was detected by immunoblotting. Actin was used as a loading control. *Lower panel* shows schematic representation of the regulation of miR-210 target gene after treatment with anti-miR-210 and siIRP1. Because the expression of IRP1 was suppressed by siRNA, there is no influence on the TfR expression by *Indirect pathway* (*gray box*). On the other hand, the expression of miR-210 was down-regulated by anti-miR-210. As a result, TfR was up-regulated in this experiment.

psi-TfR_mut, which has a mutated sequence of a putative miR-210-binding site or psi-TfR_del, which has deleted a putative miR-210-binding site. Co-transfection of pre-miR-210 down-regulated *Renilla* luciferase activity significantly more than in pre-NC in the presence of psi-TfR. In contrast, *Renilla* luciferase activity was not altered in the presence of psi-TfR_del or psi-TfR_mut (Fig. 2E). We confirmed that miR-210 targets the 3′-UTR of TfR mRNA, showing that miR-210 directly sup-

presses not only ISCU but also TfR. TfR plays a major role in cellular iron uptake through binding to and internalizing a carrier protein transferrin (Tf). Therefore, to examine whether reduction of TfR by transfected pre-miR-210 functionally inhibited the uptake of Tf or not, Alexa Fluor 594-labeled Tf was used to monitor the uptake of Tf by immunostaining and FACS analysis. As shown in Fig. 2, *F* and *G*, uptake of Tf was lower in pre-miR-210-transfected cells than in control cells,
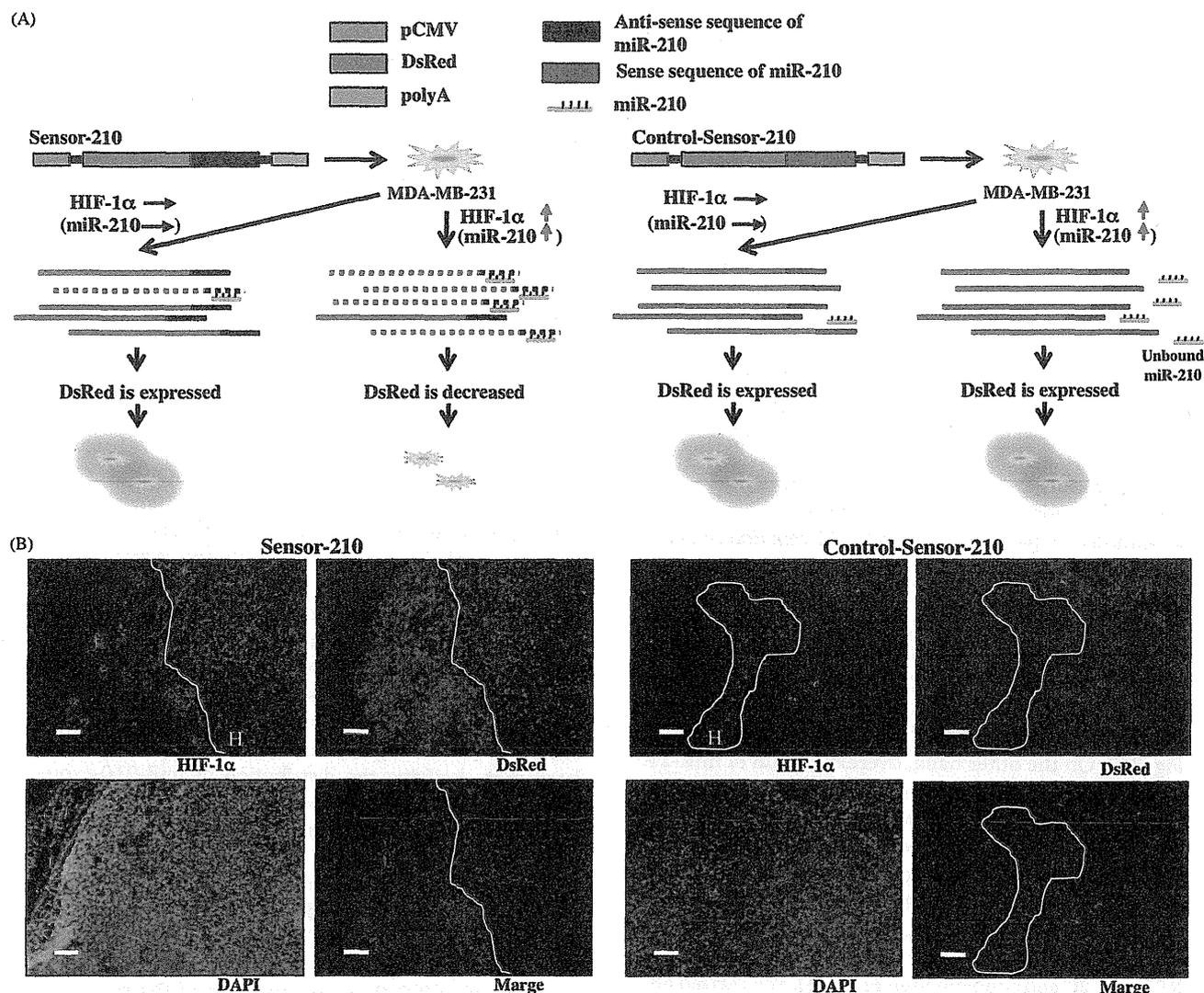
FIGURE 4. **miR-210-expressing cells were localized in the chronic hypoxic region of inoculated tumor cells.** *A,* schematic represents miR-210 tracing assay. In the hypoxic condition, expression of miR-210 is increased by the HIF-1, and then the transcripts of DsRed are degraded by miR-210 (*dashed lines with red and black*). On the other hand, expression of miR-210 is not changed under the normoxic condition (*lines with red and black*). In addition, the fluorescence of Control-Sensor-210 was not changed even under hypoxic conditions. Because their miR-210-binding sites were inserted inversely, the miR-210 could not bind to the 3'-UTR of DsRed. *B,* immunohistochemical analysis of DsRed in the tumor is shown. Sections were stained with the rabbit polyclonal anti-red fluorescent protein antibody and the mouse monoclonal anti-HIF-1α antibody. The fluorescence of DsRed could not be observed in HIF-1α-positive regions in the Sensor-210-inoculated tumor; on the other hand, there was uniform fluorescence of DsRed in Control-Sensor-210-cells-inoculated tumor. *H,* hypoxic region in a tumor is indicated. *Scale bar,* 100 μm.

indicating a direct correlation between TfR reduction and the decreased uptake of Tf in miR-210-overexpressing cells (Fig. 2, *F* and *G*). We also confirmed similar results using an MM231 cells (supplemental Fig. S4, *B* and *C*). Consequently, these observations indicated that overexpression of miR-210 decreases the concentration of intracellular iron by inhibiting the Tf-TfR-dependent iron-uptake system.

miR-210 Is a Member of Iron Homeostatic Networks—As shown in Fig. 2, overexpression of miR-210 inhibited the uptake of Tf via the suppression of TfR. However, because overexpression of miR-210 by miR-210 mimics transduces an extremely high amount of miRNA in the cells (supplemental Fig. S3*A*), it is necessary to examine the function of miR-210 in iron homeostasis under physiological conditions. To evaluate the physio-

logical relationship among miR-210, ISCU, and TfR expression, we transfected antisense miR-210 oligonucleotide (anti-miR-210), which suppresses the expression of miR-210 (supplemental Fig. S3*B*) and control oligonucleotide (anti-NC) into MCF7 cells under a hypoxic condition. We observed the induction of ISCU expression level after the transfection of anti-miR-210 (Fig. 1*F* and supplemental Fig. S2*D*); however, the expression of TfR was not affected (Fig. 3*A* and supplemental Fig. S5*A*). The knockdown of ISCU has been known to increase the expression of TfR by activating IRP1 activity (Fig. 2*C*) (26). From these observations, we assumed that unchanged TfR expression after the transfection of anti-miR-210 was caused by the up-regulation of the ISCU expression level by anti-miR-210 (Fig. 3*B*), leading to the inhibition of IRP1 activity without affecting the
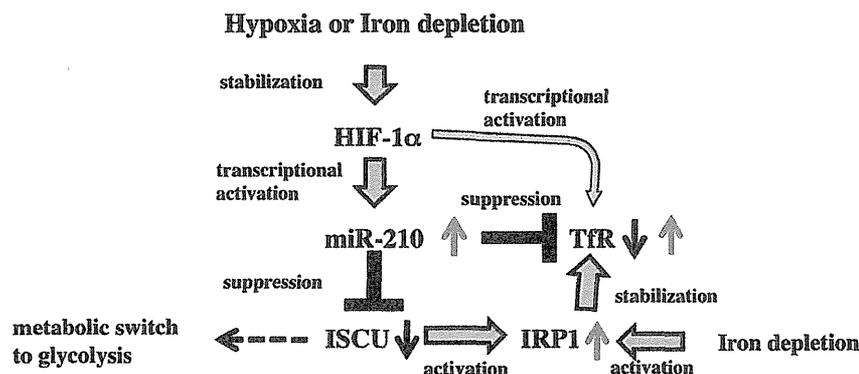
Hypoxia or Iron depletion

FIGURE 5. **Schematic representation of our proposed model.** miR-210 is induced by hypoxia and iron depletion and directly suppresses two iron homeostasis-related proteins. miR-210 regulates the iron homeostasis with dual pathways of regulating TfR expression. The *gray arrows* indicate up-regulation, and the *black arrows* indicate down-regulation. The *dashed arrow* indicates shift to metabolic switch.

IRP1 expression level. To confirm the change of IRP1 activity by miR-210 expression level in our experiment, we transfected anti-miR-210 or pre-miR-210 into MCF7 cells and analyzed the expression level of ferritin protein, which is the iron storage protein, by immunoblotting. Because the 5′-UTR of ferritin mRNA contains a single iron-responsive element that affects translation initiation, inhibition of IRP1 activity led to the up-regulation of ferritin expression (29). Indeed, the expression level of ferritin was increased in anti-miR-210-transfected cells compared with that in anti-NC-transfected cells (Fig. 3C). On the other hand, overexpression of miR-210 by pre-miR-210 suppressed the expression of ferritin in MCF7 cells, indicating that the activity of IRP1 was modulated by miR-210 through ISCU pathway (supplemental Fig. S5B). To eliminate the effect of ISCU on TfR expression in this assay system, we established stable ISCU knockdown cell lines using the MCF7 cell. In ISCU knockdown cells, the expression of TfR was higher than that in control cells by activated IRP1 (Fig. 2C and supplemental Fig. S2E). We carried out the same experiment as shown in Fig. 3A using ISCU knockdown cell lines and observed that anti-miR-210 increased TfR mRNA and protein level in ISCU knockdown cell lines but not in control cell lines (Fig. 3D). This result indicated that the expression of TfR was up-regulated by not only the down-regulation of miR-210 that directly target the TfR but also the activated IRP1, which is usually inactivated by ISCU. Furthermore, MCF7 cells were transfected with siRNA against IRP1 (or siNC) and anti-miR-210 (or anti-NC) under hypoxic condition, and these cells were analyzed for the expression of IRP1 and TfR by immunoblotting. As a result, because the IRP1 is known to stabilize the TfR mRNA, knockdown of IRP1 by siRNA caused a decrease in the expression of TfR (Fig. 3E; compare *lanes 1* and *2*). Importantly, co-transfection of anti-miR-210 and IRP1 siRNA induced the expression of TfR, indicating that miR-210 directly targets the TfR in cancer cells (Fig. 3E; compare *lanes 2* and *4*). Taken together, these data suggest that miR-210 regulates TfR expression through direct and indirect translational regulatory mechanisms to fine-tune the iron homeostasis (Fig. 3B).

The Distribution of miR-210-expressing Cells Is Associated with Chronic Hypoxia—Most tumors have lower median O_2 partial pressures than their tissue of origin and are deprived of nutrients, including iron (30). Significant variations in these relevant parameters must be expected between different locations within the same tumor at the same location at different times and between individual tumors of the same grading and staging. Previous results have shown that the expression of miR-210 is modulated by the cellular iron concentration and oxygen tension; however, what kinds of cells *in vivo* expressed miR-210 have not been clarified yet. For this reason, we postulated that clarifying the distribution of miR-210-expressing cells in the tumor leads to the understanding of cancer metabolism regulated by iron concentration. To answer this, we investigated the distribution of miR-210-expressing cells in an *in vivo* breast tumor xenograft model. In this experiment, we prepared the cell line, called MDA-MB-231-miR-210-sensor, to trace the expression of miRNA-210 *in vivo*. Because this cell was established by DsRed harboring a complementary sequence of miR-210, the fluorescence of DsRed was diminished when the expression of miR-210 was induced (Fig. 4A and supplemental Fig. S6A). We injected 5×10^6 MDA-MB-231-miR-210-sensor cells into nude mice. Prior to the excision of tumors, the mice were administered pimonidazole, a compound that binds irreversibly to hypoxic cells (31). Serial sections of the tumors were subsequently stained for pimonidazole, HIF-1α, and DsRed. A correlation between HIF-1α-positive cells and DsRed-negative cells, indicative of diminishment of DsRed expression by miR-210, was observed at the hypoxic rim around necrotic regions of the tumor, a location typically associated with chronic hypoxia (Fig. 4B). We also observed that pimonidazole-positive cells and DsRed-negative cells overlapped. On the other hand, fluorescence of control-miR-210-sensor cells, whose miR-210-binding site was inserted inversely with the miR-210-sensor vector, was not changed in inoculated tumor cells. Furthermore, we also established a cell line that enabled us to trace the expression of miR-210 by its promoter-driven DsRed (Fig. S6B) and obtained similar results with the MDA-MB-231-miR-210-sensor (Fig. S6C). Together, these observations indicated that the expression of miR-210 was

increased in the severely hypoxic region of the tumor. Namely, miR-210 regulates the iron homeostasis in cancer cells under the chronic hypoxic condition in tumors.

DISCUSSION

Iron is indispensable for the function of many prosthetic groups, whereas excess free iron can oxidize and damage the protein, nucleic acid, and lipid contents of cells. Thus, animals evolved complex mechanisms to control the favorable concentrations of intracellular iron. In this study, we revealed that miR-210 is involved in a novel iron homeostasis mechanism through the association of ISCU and TfR in cancer cells (Fig. 5). miR-210 down-regulates ISCU and the Fe-S cluster to mediate the energy metabolic shift from aerobic oxidative phosphorylation to anaerobic glycolysis (32). Concurrently, reduction of the Fe-S cluster activates IRP1, and, subsequently, the expression of TfR is increased, resulting in the elevated uptake of the iron ion. However, several reports show that the excess iron can be toxic (4). To reduce the cellular iron concentration, miR-210 directly suppresses the expression of TfR. Thus, miR-210 regulates iron homeostasis and avoids intracellular iron toxicity.

Compared with normal cells, cancer cells require a large amount of iron; thus, they generally proliferate at a larger rate than their normal counterparts. Hence, iron chelators exert their anti-proliferative effects on tumors (12). Moreover, a previous report showed that down-regulation of TfR decreased cellular proliferation and altered expression of genes involved in cell cycle control (33). Thus, as summarized in Fig. 5, it is postulated that miR-210 has two pathways for the regulation of TfR expression. One is the TfR up-regulation pathway via suppression of ISCU (indirect pathway), and the other one is the TfR down-regulation pathway by direct binding to TfR mRNA. Reduction of ISCU only increases the binding activity of IRP1, but its level of expression does not change. Thus, the effect of up-regulation of TfR by reduced ISCU depends on the amount of IRP1 protein. There are limitations to the up-regulation of TfR by the indirect pathway. Then, in the case of a further increase of miR-210, direct suppression of TfR is superior to its up-regulation by the indirect pathway. In other words, because the forced expression of miR-210 overwhelms the indirect pathway, the direct pathway is superior to the indirect one. Therefore, exogenous transfection of miR-210 causes TfR suppression (Fig. 2), thereby reducing cellular proliferation (supplemental Fig. S7) (34, 35). Moreover, we confirmed the overlap of chronic hypoxic regions and miR-210-expressing cells in inoculated cancer cells *in vivo*. These observations suggest that precise regulation of miR-210 expression level is vital for maintaining the iron homeostasis, leading to the survival and proper cellular proliferation of cancer cells.

HIFs and IRPs are key mediators of cellular iron homeostasis and oxygen, respectively. Because iron and oxygen are often intimately connected in their metabolism, it is not surprising that their levels are coordinately regulated in cells. Such crosstalk is achieved in part by cellular regulatory factors that sense and respond to both iron and oxygen, and it is reinforced by the overlap in the gene targets regulated by each pathway. For instance, binding of IRPs protects TfR mRNA from degradation, and HIF-1α activates TfR gene transcription (36, 37). In addition, in this study, we identified that hypoxia-inducible miR-210 was a key component of this pathway.

As noted above, we have clearly shown that iron homeostasis is micromanaged by miRNAs. Therefore, miRNAs could be essential for maintaining other metal homeostasis in mammals; for example, copper, zinc, and cadmium. In agreement with our observations, the current view on the molecular understanding of miRNA-guided regulation of plant heavy metal adaption was reported (38, 39). Dysregulation of metal homeostasis-related miRNAs may contribute to various diseases including cancers, nephropathy, and autoimmune disease. Further analyses are required on how these miRNAs can be affected by genetic and epigenetic mechanisms in the physiological and pathological microenvironments.

REFERENCES

1. Que, L., Jr., and Ho, R. Y. (1996) Dioxygen activation by enzymes with mononuclear nonheme iron active sites. *Chem. Rev.* 96, 2607–2624
2. Pau, M. Y., Lipscomb, J. D., and Solomon, E. I. (2007) Substrate activation for O_2 reactions by oxidized metal centers in biology. *Proc. Natl. Acad. Sci. U.S.A.* 104, 18355–18362
3. Hegg, E. L., and Que, L., Jr. (1997) The 2-His-1-carboxylate facial triad: an emerging structural motif in mononuclear nonheme iron(II) enzymes. *Eur. J. Biochem.* 250, 625–629
4. Stadtman, E. R. (1990) Metal ion-catalyzed oxidation of proteins: biochemical mechanism and biological consequences. *Free Radic. Biol. Med.* 9, 315–325
5. Clark, S. F. (2009) Iron-deficiency anemia: diagnosis and management. *Curr. Opin. Gastroenterol.* 25, 122–128
6. Raja, K. B., Duane, P., and Peters, T. J. (1990) Effects of turpentine-induced inflammation on the hypoxic stimulation of intestinal Fe^{3+} absorption in mice. *Int. J. Exp. Pathol.* 71, 785–789
7. Laftah, A. H., Raja, K. B., Latunde-Dada, G. O., Vergi, T., McKie, A. T., Simpson, R. J., and Peters, T. J. (2005) Effect of altered iron metabolism on markers of haem biosynthesis and intestinal iron absorption in mice. *Ann. Hematol.* 84, 177–182
8. Peyssonnaux, C., Zinkernagel, A. S., Schuepbach, R. A., Rankin, E., Vaulont, S., Haase, V. H., Nizet, V., and Johnson, R. S. (2007) Regulation of iron homeostasis by the hypoxia-inducible transcription factors (HIFs). *J. Clin. Invest.* 117, 1926–1932
9. Wang, G. L., Jiang, B. H., Rue, E. A., and Semenza, G. L. (1995) Hypoxia-inducible factor 1 is a basic-helix-loop-helix-PAS heterodimer regulated by cellular O_2 tension. *Proc. Natl. Acad. Sci. U.S.A.* 92, 5510–5514
10. Wang, G. L., and Semenza, G. L. (1995) Purification and characterization of hypoxia-inducible factor 1. *J. Biol. Chem.* 270, 1230–1237
11. Campbell, J. A. (1940) Effects of precipitated silica and of iron oxide on the incidence of primary lung tumors in mice. *Br. Med. J.* 2, 275–280
12. Richardson, D. R., Kalinowski, D. S., Lau, S., Jansson, P. J., and Lovejoy, D. B. (2009) Cancer cell iron metabolism and the development of potent iron chelators as anti-tumor agents. *Biochim. Biophys. Acta* 1790, 702–717
13. Bartel, D. P. (2004) MicroRNAs: genomics, biogenesis, mechanism, and function. *Cell* 116, 281–297
14. Stefani, G., and Slack, F. J. (2008) Small noncoding RNAs in animal development. *Nat. Rev. Mol. Cell Biol.* 9, 219–230
15. Calin, G. A., and Croce, C. M. (2006) MicroRNA signatures in human cancers. *Nat. Rev. Cancer* 6, 857–866
16. Rasmussen, K. D., Simmini, S., Abreu-Goodger, C., Bartonicek, N., Di Giacomo, M., Bilbao-Cortes, D., Horos, R., Von Lindern, M., Enright, A. J.,

and O'Carroll, D. (2010) The miR-144/451 locus is required for erythroid homeostasis. *J. Exp. Med.* **207**, 1351–1358

17. Kosaka, N., Sugiura, K., Yamamoto, Y., Yoshioka, Y., Miyazaki, H., Komatsu, N., Ochiya, T., and Kato, T. (2008) Identification of erythropoietin-induced microRNAs in haematopoietic cells during erythroid differentiation. *Br. J. Haematol.* **142**, 293–300

18. Camps, C., Buffa, F. M., Colella, S., Moore, J., Sotiriou, C., Sheldon, H., Harris, A. L., Gleadle, J. M., and Ragoussis, J. (2008) HSA-miR-210 is induced by hypoxia and is an independent prognostic factor in breast cancer. *Clin. Cancer Res.* **14**, 1340–1348

19. Friedman, R. C., Farh, K. K., Burge, C. B., and Bartel, D. P. (2009) Most mammalian mRNAs are conserved targets of microRNAs. *Genome Res.* **19**, 92–105

20. Griffiths-Jones, S., Grocock, R. J., van Dongen, S., Bateman, A., and Enright, A. J. (2006) miRBase: microRNA sequences, targets, and gene nomenclature. *Nucleic Acids Res.* **34**, D140–144

21. Wang, X., and El Naqa, I. M. (2008) Prediction of both conserved and nonconserved microRNA targets in animals. *Bioinformatics* **24**, 325–332

22. Huang, X., Ding, L., Bennewith, K. L., Tong, R. T., Welford, S. M., Ang, K. K., Story, M., Le, Q. T., and Giaccia, A. J. (2009) Hypoxia-inducible miR-210 regulates normoxic gene expression involved in tumor initiation. *Mol. Cell* **35**, 856–867

23. Fujita, S., Ito, T., Mizutani, T., Minoguchi, S., Yamamichi, N., Sakurai, K., and Iba, H. (2008) miR-21 gene expression triggered by AP-1 is sustained through a double-negative feedback mechanism. *J. Mol. Biol.* **378**, 492–504

24. Burk, U., Schubert, J., Wellner, U., Schmalhofer, O., Vincan, E., Spaderna, S., and Brabletz, T. (2008) A reciprocal repression between ZEB1 and members of the miR-200 family promotes EMT and invasion in cancer cells. *EMBO Rep.* **9**, 582–589

25. Ye, H., and Rouault, T. A. (2010) Erythropoiesis and iron-sulfur cluster biogenesis. *Adv. Hematol.* **2010**, 10.1155/2010/329394

26. Tong, W. H., and Rouault, T. A. (2006) Functions of mitochondrial ISCU and cytosolic ISCU in mammalian iron-sulfur cluster biogenesis and iron homeostasis. *Cell Metab.* **3**, 199–210

27. Chen, Z., Li, Y., Zhang, H., Huang, P., and Luthra, R. (2010) Hypoxia-regulated microRNA-210 modulates mitochondrial function and decreases ISCU and COX10 expression. *Oncogene* **29**, 4362–4368

28. Favaro, E., Ramachandran, A., McCormick, R., Gee, H., Blancher, C., Crosby, M., Devlin, C., Blick, C., Buffa, F., Li, J. L., Vojnovic, B., Pires das

29. Neves, R., Glazer, P., Iborra, F., Ivan, M., Ragoussis, J., and Harris, A. L. (2010) MicroRNA-210 regulates mitochondrial free radical response to hypoxia and Krebs cycle in cancer cells by targeting iron-sulfur cluster protein ISCU. *PLoS One* **5**, e10345

29. Hentze, M. W., Caughman, S. W., Rouault, T. A., Barriocanal, J. G., Dancis, A., Harford, J. B., and Klausner, R. D. (1987) Identification of the iron-responsive element for the translational regulation of human ferritin mRNA. *Science* **238**, 1570–1573

30. Vaupel, P., Kallinowski, F., and Okunieff, P. (1989) Blood flow, oxygen and nutrient supply, and metabolic microenvironment of human tumors: a review. *Cancer Res.* **49**, 6449–6465

31. Raleigh, J. A., Chou, S. C., Arteel, G. E., and Horsman, M. R. (1999) Comparisons among pimonidazole binding, oxygen electrode measurements, and radiation response in C3H mouse tumors. *Radiat. Res.* **151**, 580–589

32. Chan, S. Y., Zhang, Y. Y., Hemann, C., Mahoney, C. E., Zweier, J. L., and Loscalzo, J. (2009) MicroRNA-210 controls mitochondrial metabolism during hypoxia by repressing the iron-sulfur cluster assembly proteins ISCU1/2. *Cell Metab.* **10**, 273–284

33. O'Donnell, K. A., Yu, D., Zeller, K. I., Kim, J. W., Racke, F., Thomas-Tikhonenko, A., and Dang, C. V. (2006) Activation of transferrin receptor 1 by c-Myc enhances cellular proliferation and tumorigenesis. *Mol. Cell. Biol.* **26**, 2373–2386

34. Chitambar, C. R., Massey, E. J., and Seligman, P. A. (1983) Regulation of transferrin receptor expression on human leukemic cells during proliferation and induction of differentiation: effects of gallium and dimethylsulfoxide. *J. Clin. Invest.* **72**, 1314–1325

35. Neckers, L. M., and Trepel, J. B. (1986) Transferrin receptor expression and the control of cell growth. *Cancer Invest.* **4**, 461–470

36. Lok, C. N., and Ponka, P. (1999) Identification of a hypoxia-response element in the transferrin receptor gene. *J. Biol. Chem.* **274**, 24147–24152

37. Tacchini, L., Bianchi, L., Bernelli-Zazzera, A., and Cairo, G. (1999) Transferrin receptor induction by hypoxia: HIF-1-mediated transcriptional activation and cell-specific post-transcriptional regulation. *J. Biol. Chem.* **274**, 24142–24146

38. Yamasaki, H., Abdel-Ghany, S. E., Cohu, C. M., Kobayashi, Y., Shikanai, T., and Pilon, M. (2007) Regulation of copper homeostasis by microRNA in Arabidopsis. *J. Biol. Chem.* **282**, 16369–16378

39. Abdel-Ghany, S. E., and Pilon, M. (2008) MicroRNA-mediated systemic down-regulation of copper protein expression in response to low copper availability in Arabidopsis. *J. Biol. Chem.* **283**, 15932–15945

Review

Secretory MicroRNAs by Exosomes as a Versatile Communication Tool

Takahiro OCHIYA

Division of Molecular and Cellular Medicine, National Cancer Center Research Institute
5–1–1 Tsukiji, Chuo-ku, Tokyo, 104–0045 Japan

Abstract: In the past several years, the importance of microRNA (miRNA) in cancer cells has been recognized. Proper control of miRNA expression is essential for maintaining a steady state of the cellular machinery. Dysregulation of miRNAs leads to the cancer development, meaning that expression profile of miRNAs can be used as cancer biomarker, and recovery of down-regulated miRNAs or inhibition of up-regulated miRNAs will be a novel approach for cancer therapy. Recently, it was discovered that extracellular miRNAs circulate in the blood of both healthy and diseased patients. Most of the circulating miRNAs are included in protein, lipid or lipoprotein complexes, such as RNA-binding proteins, apoptotic bodies, microvesicles, or exosomes, and are, therefore, highly stable. The existence of circulating miRNAs in the blood of cancer patients has raised the possibility that miRNAs may serve as a novel diagnostic marker. However, the secretory mechanism and biological function, as well as the meaning of the existence of extracellular miRNAs, remain largely unclear. Our recent study revealed the secretory mechanism of miRNAs and showed their cell-to-cell transfer. Here we summarize current approaches to modulate the intercellular and interindividual network via silencing signals exported by secretory miRNAs and discuss about the usage of circulating miRNAs as a novel communication tool.

Key words: microRNA, exosome, diagnosis, micro-environment, communication.

Finding of secreting microRNAs in body fluids

Growing evidence suggests that extracellular microRNAs (miRNAs) stably exist in human body fluids, including plasma, saliva, and urine, although ribonucleases (RNases) also circulate throughout the body.[1] This finding indicates that miRNAs are excreted after they are contained in RNase-resistant lipid vesicles, such as exosomes and apoptotic bodies. Recent studies have revealed the novel genetic exchange between cells using miRNA either in microvesicles (up to 1 μm) or in small membrane vesicles of endocytic origin called exosomes (50~100 nm).[2~11] One of the first reports showing the existence of miRNA in exosomes was studied by Valadi et al., who reported that exosomes released from human and murine mast cell lines contain mRNAs and miRNAs.[11] Hunter et al. demonstrated that miRNAs contained in the microvesicles from blood were known to regulate the cellular differentiation of blood

cells and metabolic pathways and to modulate immune function.[12] Apart from microvesicles and exosomes, more recent evidence has suggested that circulating microRNAs found in sera of the human are coupled with some specific proteins and lipoproteins. However, very little is known about the secretory machinery of miRNAs.

Oral cancer miRNAs in saliva

Considering that exosomes and microvesicles are evident in several types of body fluid from cancer patients, miRNA surely be able to be found not only in serum/plasma but also in other body fluid. Indeed, Michael et al. showed the presence of miRNAs within exosomes isolated from human saliva.[13] Furthermore, analyzing patient saliva with a polymerase chain reaction (PCR) technique, Park et al. found that miR-125a and miR-200a were present in significantly lower levels

**Significance of Exosomes/microRNAs
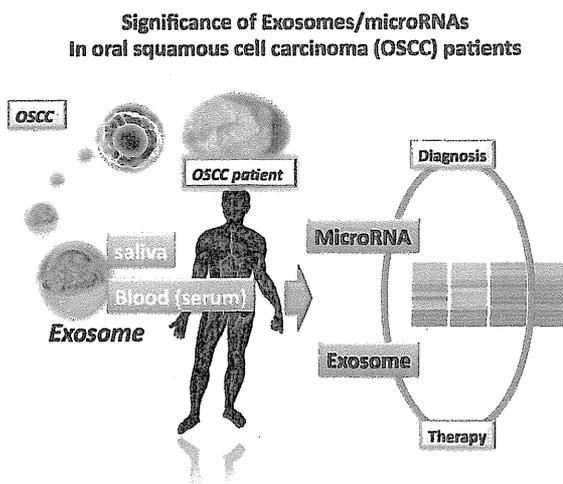In oral squamous cell carcinoma (OSCC) patients**

Fig. 1 Significance of Exosomes/microRNAs in oral squamous cell carcinoma (OSCC) patients. Circulating microRNAs in OSCC patients-exosomes (saliva and serum) are useful for a novel diagnosis and therapeutics against OSCC.

in the saliva of oral squamous cell carcinoma (OSCC) patients than in control subjects.[14] These findings suggest that the detection of miRNAs in saliva can be used as a noninvasive and rapid diagnostic tool for the diagnosis of oral cancer (Fig. 1). OSCC is the sixth most common cancer in the U.S., accounting for 90% of oral cancers and leading to 8,000 deaths per year. The average five-year survival rate for OSCC is about 50%, and this number has not changed in last three decades. Therefore, an early detection method for OSCC is needed to increase long-term patient survival. In this connection, finding of OSCC specific miRNAs highlighted a novel means of early cancer detection, and that the presence of salivary miRNA adds a third type of molecule, in addition to proteome and transcriptome, that can be measured in human saliva.

Exosomes in saliva

As human plasma, saliva contain exosomal particles. Saliva from healthy human donors was collected in tubes. For the RNA isolation, 100 μl of the protease inhibitor and RNase inhibitor were added per 20 ml of saliva. The saliva was diluted 1:1 with phosphate buffered saline (PBS) and centrifuged at 20,000×g for

20 min to remove cells and cell debris. The supernatant was filtered through a 0.2 μm filtration system and then ultracentrifugation at 100,000×g for 70 min to pellet the exosomes. By electron microscopic analysis, salivary exosomes look like round shape with 120~150 nm in a diameter. It is reported that exosomes from saliva can be taken up by human macrophages, as shown by the uptake of fluorescently stained exosomes.[15] It has been shown that other cells can take up exosomes in a similar way to macrophages, which means that this is a common feature of exosomes. It has not been determined the cellular origin of saliva exosomes, but it has been shown that primary cultures of salivary glands can release exosomes-like particles suggesting that exosomes in saliva are partly derived from salivary gland epithelial cells.

Molecular mechanisms of secreting miRNAs and exosomes

Our group demonstrated that the secretion of miRNAs depends on the cellular amount of ceramide, a bioactive sphingolipid, whose synthesis is tightly regulated by neutral sphingomyelinase 2 (nSMase2).[16] Treatment of a chemical compound, GW4869, which can inhibit the enzymatic activity of nSMase2, markedly blocked the secretion of miRNAs and exosomes. These data suggest that miRNAs are secreted by an exosome-dependent pathway that involves ceramide biosynthesis. The molecular dissection of miRNA secretory mechanisms is likely to assist in a better understanding why the expression of secretory miRNAs is perturbed during the development of various diseases, including cancer, diabetes, and immune disorders.[17~19] This finding may be beneficial to confer reliability and credibility to the diagnostic use of secretory miRNAs.

Intracellular communication by exosomes

As evidenced by many reports,[20~24] small RNAs are currently regarded as a category of intercellular signal entities, which are called, for instance, mobile small RNAs, systemic silencing signals, or just secreted RNAs. To answer the question as to whether

the secretory exosomal miRNAs that we observed can function biologically in a similar manner to other members, we set up *in vitro* and *in vivo* experiments pertaining to intercellular transfer. Purified exosomes labeled with a green fluorescent reagent PKH67 were successfully incorporated into recipient PC-3 cells. We also detected the migration of secretory nucleic acids into PC-3 cells by using SYTO dye, a specific probe for vital DNAs and RNAs including mRNAs and miRNAs. Furthermore, we reported that secretory miR-146 inducing a phenotypic change in the incorporated cells. It is generally acknowlkedged that normal epithelial cells regulate the secretion of autocrine and paracrine factors that prevent aberrant growth of neighboring cells, leading to healthy development and normal metabolism. One reason for tumor initiation is considered to be a failure of this homeostatic cell competitive system. Kosaka et al. identify tumor-suppressive miRNAs secreted by normal cells as anti-proliferative signal entities.[25] Among these miRNAs, secretory miR-143 could induce growth inhibition exclusively in cancer cells *in vitro* and *in vivo*. These results suggest that secretory tumor-suppressive miRNAs can act as a death signal in a cell competitive process. Taken together, the findings indicate that exosomal secretory miRNAs can spread translation-inhibitory signals, leading to the elicitation of a wide array of biological events.

Secretory miRNAs could be an interindividual communication tool

The relevance of miRNA transfer cannot be limited within an individual organism. Kosaka et al. found that the expression of immune-related miRNAs in human breast milk culminates in the first 6 months of lactation, in agreement with the significance of colostrum in the context of passive immunity.[26] This paper appears to suggest the two important concepts such as dietary intake of miRNAs and vertical transfer of miRNAs. If the miRNAs intake by daily food maintain their biological activity after digestion, they will be highly valued as a crucial ingredient that can modulate gene expression

of our own cells. In fact, current reports suggested that plant (rice origin) miRNAs could found in the circulating blood.[27] The microRNAs seem to come from ingested rice. Presumably the micoRNAs are taken up in the intestine and secreted into the blood in small vesicles, since microRNAs packaged into exosomes are highly stable in low pH such as stomach acid. Based on the second concept, genetic exchanges between mother and child would be mediated by milk-exosomes as well as amniotic fluids. The excretions from the body, such as tears, saliva, semen, and vaginal discharge, also include secretory miRNAs, suggesting that these fluids may act as a mediator of horizontal genetic materials transfer. It is within the bounds of probability that secretory miRNAs could be an interindividual communication tool among humans.

Perspective

The existence of circulating miRNAs and micro-vesicles in the blood of cancer patients has raised the possibility that disease-specific miRNAs and exosomes may serve as a novel diagnostic marker. Moreover, exosomes secreted from tumor cells contribute maicro-managing tumor microenvironment. Intracellular communications via microRNAs and microvesicles including exosomes are important novel therapeutic targets for inhibiting tumor development and metastasis including oral cancer.

References

1) Kosaka N, Iguchi H, Ochiya T: Circulating microRNA in body fluid: a new potential biomarker for cancer diagnosis and prognosis. Cancer Sci, 101: 2087–2092, 2010

2) Cocucci E, Racchetti G, Meldolesi J: Shedding microvesicles: artefacts no more. Trends Cell Biol, 19: 43–51, 2009

3) Ghosh AK, Secreto CR, Knox TR, Ding W, Mukhopadhyay D, Kay NE: Circulating microvesicles in B-cell chronic lymphocytic leukemia can stimulate marrow stromal cells: implications for disease progression. Blood, 115: 1755–1764, 2010

4) Lima LG, Chammas R, Monteiro RQ, Moreira ME, Barcinski MA: Tumor-derived microvesicles modulate the establishment of metastatic melanoma in a phosphatidylserine-dependent manner. Cancer Lett, 283: 168–175, 2009

5) Skog J, Wurdinger T, van Rijn S, Meijer DH, Gainche L, Sena-Esteves M, Curry WT, Jr., Carter BS, Krichevsky AM, Breakefield XO: Glioblastoma microvesicles transport RNA and proteins that promote tumour growth and provide diagnostic biomarkers. Nat Cell Biol, 10: 1470–1476, 2008

6) Wolfers J, Lozier A, Raposo G, Regnault A, Thery C, Masurier C, Flament C, Pouzieux S, Faure F, Tursz T, Angevin E, Amigorena S, Zitvogel L: Tumor-derived exosomes are a source of shared tumor rejection antigens for CTL cross-priming. Nat Med, 7: 297–303, 2001

7) Burden HP, Holmes CH, Persad R, Whittington K: Prostasomes—their effects on human male reproduction and fertility. Hum Reprod Update, 12: 283–292, 2006

8) Babiker AA, Nilsson B, Ronquist G, Carlsson L, Ekdahl KN: Transfer of functional prostasomal CD59 of metastatic prostatic cancer cell origin protects cells against complement attack. Prostate, 62: 105–114, 2005

9) Holmgren L, Szeles A, Rajnavolgyi E, Folkman J, Klein G, Ernberg I, Falk KI: Horizontal transfer of DNA by the uptake of apoptotic bodies. Blood, 93: 3956–3963, 1999

10) Zernecke A, Bidzhekov K, Noels H, Shagdarsuren E, Gan L, Denecke B, Hristov M, Koppel T, Jahantigh MN, Lutgens E, Wang S, Olson EN, Schober A, Weber C: Delivery of microRNA-126 by apoptotic bodies induces CXCL12-dependent vascular protection. Sci Signal, 2: ra81, 2009

11) Valadi H, Ekstrom K, Bossios A, Sjostrand M, Lee JJ, Lotvall JO: Exosome-mediated transfer of mRNAs and microRNAs is a novel mechanism of genetic exchange between cells. Nat Cell Biol, 9: 654–659, 2007

12) Hunter MP, Ismail N, Zhang X, Aguda BD, Lee EJ, Yu L, Xiao T, Schafer J, Lee ML, Schmittgen TD, Nana-Sinkam SP, Jarjoura D, Marsh CB: Detection of microRNA expression in human peripheral blood microvesicles. PLoS One, 3: e3694, 2008

13) Michael A, Bajracharya, SD, Yuen PS, Zhou H, Star RA, Illei GG, Alevizos I: Exosomes from human saliva as a source of microRNA biomarkers. Oral Dis, 16: 34–38, 2010

14) Park NJ, Zhou H, Elashoff D, Henson BS, Kastratovic DA, Abemayor E, Wong DT: Salivary microRNA: discovery, characterization, and clinical utility for oral cancer detection. Clin Cancer Res, 15: 5473–5477, 2009

15) Lässer C, Alikhani VS, Ekström K, Eldh M, Paredes PT, Bossios A, Sjöstrand M, Gabrielsson S, Lötvall J, Valadi H: Human saliva, plasma and breast milk exosomes contain RNA: uptake by macrophages. J Transl Med, 9: 9, 2011

16) Kosaka N, Iguchi H, Yoshioka Y, Takeshita F, Matsuki Y, Ochiya T: Secretory mechanisms and intercellular transfer of MicroRNAs in living cells. J Biol Chem, 285: 17442–17452, 2010

17) Chen X, Ba Y, Ma L, Cai X, Yin Y, Wang K, Guo J, Zhang Y, Chen J, Guo X, Li Q, Li X, Wang W, Zhang Y, Wang J, Jiang X, Xiang Y, Xu C, Zheng P, Zhang J, Li R, Zhang H, Shang X, Gong T, Ning G, Wang J, Zen K, Zhang J, Zhang CY: Characterization of microRNAs in serum: a novel class of biomarkers for diagnosis of cancer and other diseases. Cell Res, 18: 997–1006, 2008

18) Lawrie CH, Gal S, Dunlop HM, Pushkaran B, Liggins AP, Pulford K, Banham AH, Pezzella F, Boultwood J, Wainscoat JS, Hatton CS, Harris AL: Detection of elevated levels of tumour-associated microRNAs in serum of patients with diffuse large B-cell lymphoma. Br J Haematol, 141: 672–675, 2008

19) Murata K, Yoshitomi H, Tanida S, Ishikawa M, Nishitani K, Ito H, Nakamura T: Plasma and synovial fluid microRNAs as potential biomarkers of rheumatoid arthritis and osteoarthritis. Arthritis Res Ther, 12: R86, 2010

20. Dunoyer P, Schott G, Himber C, Meyer D, Takeda A, Carrington JC, Voinnet O: Small RNA duplexes function as mobile silencing signals between plant cells. Science, 328: 912–916, 2010

21) Mlotshwa S, Voinnet O, Mette MF, Matzke M, Vaucheret H, Ding SW, Pruss G, Vance VB: RNA silencing and the mobile silencing signal. Plant Cell, 14 (Suppl): S289–S301, 2002

22) Molnar A, Melnyk CW, Bassett A, Hardcastle TJ, Dunn R, Baulcombe DC: Small silencing RNAs in plants are mobile and direct epigenetic modification in recipient cells. Science, 328: 872–875, 2010

23) Pegtel DM, Cosmopoulos K, Thorley-Lawson DA, van Eijndhoven MA, Hopmans ES, Lindenberg JL, de Gruijl TD, Wurdinger T, Middeldorp JM: Functional delivery of viral miRNAs via exosomes. Proc Natl Acad Sci USA, 107: 6328–6333, 2010

24) Zernecke A, Bidzhekov K, Noels H, Shagdarsuren E, Gan L, Denecke B, Hristov M, Koppel T, Jahantigh MN, Lutgens E, Wang S, Olson EN, Schober A, Weber C: Delivery of microRNA-126 by apoptotic bodies induces CXCL12-dependent vascular protection. Sci Signal, 2: ra81, 2009

25) Kosaka N, Iguchi H, Yoshioka Y, Hagiwara K, Takeshita F, Ochiya T: Competitive interactions of cancer cells and normal cells via secretory microRNAs. J Biol Chem, 287: 1397–1405, 2012

26) Kosaka N, Izumi H, Sekine K, Ochiya T: microRNA as a new immune-regulatory agent in breast milk. Silence, 1: 7, 2010

27) Zhang L, Hou D, Chen X, Li D, Zhu L, Zhang Y, Li J, Bian Z, Liang X, Cai X, Yin Y, Wang C, Zhang T, Zhu D, Zhang D, Xu J, Chen Q, Ba Y, Liu J, Wang Q, Chen J, Wang J, Wang M, Zhang Q, Zhang J, Zen K, Zhang CY: Exogenous plant MIR168a specifically targets mammalian LDLRAP1: evidence of cross-kingdom regulation by microRNA. Cell Res, 22: 107–26, 2012

Article

Genome-Wide Analysis of DNA Methylation and Expression of MicroRNAs in Breast Cancer Cells

Sumiyo Morita [1], **Ryou-u Takahashi** [2], **Riu Yamashita** [3], **Atsushi Toyoda** [4], **Takuro Horii** [1], **Mika Kimura** [1], **Asao Fujiyama** [4], **Kenta Nakai** [5], **Shoji Tajima** [6], **Ryo Matoba** [7], **Takahiro Ochiya** [2] **and Izuho Hatada** [1,*]

[1] Laboratory of Genome Science, Biosignal Genome Resource Center, Institute for Molecular and Cellular Regulation, Gunma University, Gunma 371-8512, Japan;
E-Mails: msumiyo@gunma-u.ac.jp (S.M.); horii@gunma-u.ac.jp (T.H.); mikimura@showa.gunma-u.ac.jp (M.K.)

[2] Division of Molecular and Cellular Medicine, National Cancer Center Research Institute, 5-1-1, Tsukiji, Chuo-ku, Tokyo 104-0045, Japan; E-Mails: rytakaha@ncc.go.jp (R.T.); tochiya@ncc.go.jp (T.O.)

[3] Department of Integrative Genomics, Medical Megabank Organization, Tohoku University, 6-3-09, aza Aoba, Aramaki, Aobaku, Sendai 980-8579, Japan; E-Mail: ryamasi@megabank.tohoku.ac.jp

[4] Center for Genetic Resource Information, National Institute of Genetics, Shizuoka 411-8540, Japan; E-Mails: atoyoda@lab.nig.ac.jp (A.T.); afujiyam@lab.nig.ac.jp (A.F.)

[5] Human Genome Center, Institute of Medical Science, University of Tokyo, 4-6-1 Shirokanedai, Minato-ku, Tokyo 108-8639, Japan; E-Mail: knakai@ims.u-tokyo.ac.jp

[6] Laboratory of Epigenetics, Institute for Protein Research, Osaka University, 3-2 Yamadaoka, Suita, Osaka 565-0871, Japan; E-Mail: tajima@protein.osaka-u.ac.jp

[7] DNA Chip Research Inc., 1-1-43 Suehirocho, Tsurumi-ku, Yokohama, Kanagawa 230-0045, Japan; E-Mail: matoba@dna-chip.co.jp

* Author to whom correspondence should be addressed; E-Mail: hatada@gunma-u.ac.jp; Tel.: +81-27-220-8057; Fax: +81-27-220-8110.

Abstract: DNA methylation of promoters is linked to transcriptional silencing of protein-coding genes, and its alteration plays important roles in cancer formation. For example, hypermethylation of tumor suppressor genes has been seen in some cancers. Alteration of methylation in the promoters of microRNAs (miRNAs) has also been linked to transcriptional changes in cancers; however, no systematic studies of methylation and